Advances in Detector Technologies for Visible and Infrared Wavefront Sensing

Philippe Feautrier[ai,1], Jean-Luc Gach[bi], Mark Downing[c], Paul Jorden[d], Johann Kolb[c], Johan Rothman[e], Thierry Fusco[f], Philippe Balard[bi], Eric Stadler[ai], Christian Guillaume[gi], David Boutolleau[i], Gérard Destefanis[e], Nicolas Lhermet[e], Olivier Pacaud[j], Michel Vuillermet[j], Alexandre Kerlain[j], Norbert Hubin[c], Javier Reyes[c], Markus Kasper[c], Olaf Ivert[c], Wolfgang Suske[d], Andrew Walker[d], Michael Skegg[d], Sophie Derelle[k], Joel Deschamps[k], Clélia Robert[f] , Nicolas Vedrenne[f] , Frédéric Chazalet[l], Julien Tanchon[m], Thierry Trollier[m], Alain Ravex[m], Gérard Zins[a], Pierre Kern[a], Thibaut Moulin[a] and Olivier Preis[a].

[a]Institut de Planétologie et d'Astrophysique de Grenoble, UJF-Grenoble 1, CNRS-INSU, Domaine Universitaire, 414 rue de la Piscine, BP 53 38041 Grenoble Cedex 9, France;
[b]LAM, Laboratoire d'Astrophysique de Marseille, Technopôle de Château-Gombert - 38, rue Frédéric Joliot-Curie -13388 Marseille, France;
[c]ESO, Karl-Schwarzschild-Strasse 2, 85748 Garching bei München, Germany;
[d]e2v technologies,106 Waterhouse Lane, Chelmsford, Essex, CM1 2QU, England;
[e]CEA/LETI - Minatec Campus - 17 rue des Martyrs - 38054 Grenoble Cedex 9- France
[f]ONERA, 29 avenue de la Division Leclerc, BP 72, 92322 Chatillon Cedex, France;
[g]OHP, Observatoire de Haute Provence, 04870 St.Michel l'Observatoire, France;
[i]First Light Imaging, Hôtel Technoptic, Rue Marc Donadille, 13388 Marseille cedex 13, France;
[j]SOFRADIR, 43-47 rue Camille Pelletan, 92290 Châtenay-Malabry, France;
[k]ONERA, Chemin de la Hunière, 91123 Palaiseau Cedex, France;
[l]SHAKTI, 27 bd Charles Moretti, Bât B, 13 014 Marseille, France;
[m]Absolut Systems, 32 rue de la Tuilerie, 38170 Seyssinet-Pariset, France.

ABSTRACT

The purpose of this paper is to give an overview of the state of the art wavefront sensor detectors developments held in Europe for the last decade.

The success of the next generation of instruments for 8 to 40-m class telescopes will depend on the ability of Adaptive Optics (AO) systems to provide excellent image quality and stability. This will be achieved by increasing the sampling, wavelength range and correction quality of the wave front error in both spatial and time domains.

The modern generation of AO wavefront sensor detectors development started in the late nineties with the CCD50 detector fabricated by e2v technologies under ESO contract for the ESO NACO AO system. With a 128x128 pixels format, this 8 outputs CCD offered a 500 Hz frame rate with a readout noise of 7e-.

A major breakthrough has been achieved with the recent development by e2v technologies of the CCD220. This 240x240 pixels 8 outputs EMCCD (CCD with internal multiplication) has been jointly funded by ESO and Europe under the FP6 programme. The CCD220 and the OCAM2 camera that operates the detector are now the most sensitive system in the world for advanced adaptive optics systems, offering less than 0.2 e readout noise at a frame rate of 1500 Hz with negligible dark current. Extremely easy to operate, OCAM2 only needs a 24 V power supply and a modest water cooling

[1] Contact address: philippe.feautrier@obs.ujf-grenoble.fr

circuit. This system, commercialized by First Light Imaging, is extensively described in this paper. An upgrade of OCAM2 is foreseen to boost its frame rate to 2 kHz, opening the window of XAO wavefront sensing for the ELT using 4 synchronized cameras and pyramid wavefront sensing.

Since this major success, new developments started in Europe. One is fully dedicated to Natural and Laser Guide Star AO for the E-ELT with ESO involvement. The spot elongation from a LGS Shack Hartman wavefront sensor necessitates an increase of the pixel format. Two detectors are currently developed by e2v. The NGSD will be a 880x840 pixels CMOS detector with a readout noise of 3 e (goal 1e) at 700 Hz frame rate. The LGSD is a scaling of the NGSD with 1760x1680 pixels and 3 e readout noise (goal 1e) at 700 Hz (goal 1000 Hz) frame rate. New technologies will be developed for that purpose: advanced CMOS pixel architecture, CMOS back thinned and back illuminated device for very high QE, full digital outputs with signal digital conversion on chip. In addition, the CMOS technology is extremely robust in a telescope environment. Both detectors will be used on the European ELT but also interest potentially all giant telescopes under development.

Additional developments also started for wavefront sensing in the infrared based on a new technological breakthrough using ultra low noise Avalanche Photodiode (APD) arrays within the RAPID project. Developed by the SOFRADIR and CEA/LETI manufacturers, the latter will offer a 320x240 8 outputs 30 microns IR array, sensitive from 0.4 to 3.2 microns, with 2 e readout noise at 1500 Hz frame rate. The high QE response is almost flat over this wavelength range. Advanced packaging with miniature cryostat using liquid nitrogen free pulse tube cryocoolers is currently developed for this programme in order to allow use on this detector in any type of environment. First results of this project are detailed here.

These programs are held with several partners, among them are the French astronomical laboratories (LAM, OHP, IPAG), the detector manufacturers (e2v technologies, Sofradir, CEA/LETI) and other partners (ESO, ONERA, IAC, GTC). Funding is: Opticon FP6 and FP7 from European Commission, ESO, CNRS and Université de Provence, Sofradir, ONERA, CEA/LETI and the French FUI (DGCIS).

Keywords: Adaptive optics, Electron Multiplying CCD, EMCCD, L3Vision CCD, Avalanche photodiodes, HgCdTe, low readout noise, wavefront sensor, sub-electron noise.

1. OCAM AND THE CCD220

1.1 Introduction

The success of the next generation of ESO (European Southern Observatory) instruments [1] for 8 to 10-m class telescopes will depend on the ability of Adaptive Optics (AO) systems to provide excellent image quality and stability. This will be achieved by increasing the sampling and correction of the wave front error in both spatial and time domains. For example, advanced Shack Hartmann systems currently fabricated require 40x40 sub-apertures at sampling rates of 1-1.5 kHz as opposed to 14x14 sub-apertures at 500 Hz of previous AO systems. Beyond the e2v CCD50 developed for the ESO NACO instrument in the late nineties [2], new detectors of 240x240 pixels are required to provide the spatial dynamics of 5-6 pixels per sub-aperture. Higher temporal-spatial sampling implies fewer photons per pixel therefore the need for much lower read noise (<<1e-) and negligible dark current (<< 1e-/pixel/frame) to detect and centroid on a small number of photons

The detector development described in this paper was jointly funded by ESO and the OPTICON European network [3] in the Joint Research Activity JRA2 [4], “Fast Detectors for Adaptive Optic". *e2v technologies* [5] was chosen in 2005 to develop a dedicated detector based on an extension of their L3Vision [6] EMCCD technology. Analysis [7] showed that the sub-electron read noise of L3Vision CCDs clearly outperformed classical CCDs even though L3Vision devices exhibit the excess noise factor F of $2^{1/2}$ typical of EMCCDs [8], [9], [10].

1.2 The CCD220 design

The CCD220 was the name chosen by *e2v technologies* for this detector. The CCD220 [11], [12], [13], [14], [15], [16], [17] (schematic in Figure 1) is a 24 µm square 240x240 pixels split frame transfer back illuminated L3Vision CCD. The image and store area (store is optically shielded) are built with 2-phase metal-buttressed parallel clock structures to enable fast line shifts in excess of 7 Mlines/s for total transfer time from image to store of 18 µs and low smearing of under 2% at 1200 fps. Eight Electron-Multiplying [6] registers operating at greater than 13 Mpixel/sec enable sub electron noise to be achieved at frame rates of 1300 fps.

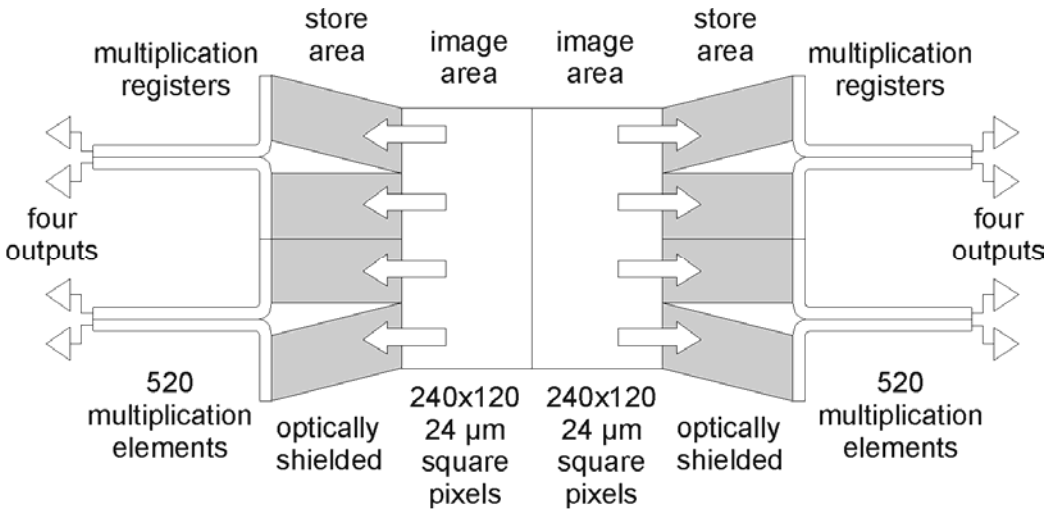

Figure 1: Schematic of e2v technologies 240x240 pixel L3Vision CCD220. Eight Electron-Multiplying (gain) registers are used to obtain sub-electron noise at frame rates of 1300 fps.

The CCD220 is encapsulated in a 64 pin package (see Figure 2) with a custom-designed integral Peltier cooler that cools down the CCD below -45°C to achieve the required total dark current. The package is sealed and back-filled with 0.9 bar of Krypton gas to minimize heat transfer to the outside. Extensive thermal modeling [18] of the CCD, Peltier cooler, package, proposed clamping arrangement and water-cooled heat exchanger was performed. The modeling results which have been verified by measurement show that for 10 °C water temperature in the heat exchanger, the Peltier can cool the CCD to below -45 °C. This enables the dark current specification (<0.01 e/pix/frame at 1300 fps and <0.04 e/pix/frame at 25 fps) of the standard silicon device to be easily achieved.

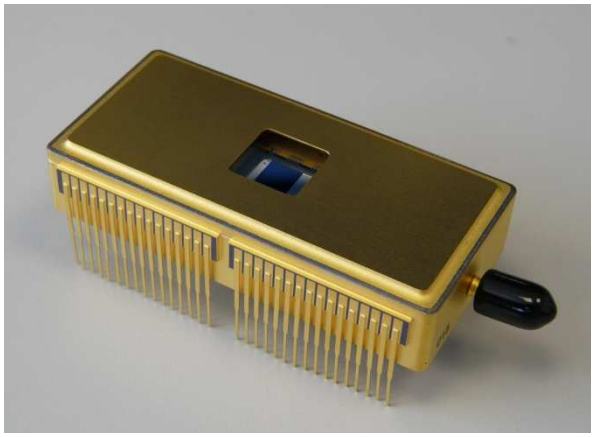

Figure 2. Photograph of CCD220 package with integral Peltier cooler that has been verified (first by thermal modeling then by measurement) to cool the CCD below -45°C to achieve < 0.01 e-/pix/frame total dark current.

1.3 The OCAM2 Camera

OCAM2, the production version of the OCam test camera, is commercialized by First Light Imaging [19].Whereas OCam has been designed to test CCDs and provides many tuning capabilities (voltages, features and so-on), OCAM2 is a ready-to-use camera with embedded parameters to run the CCD, factory optimised. OCAM2 has also been designed for ruggedness and can cope with more demanding environmental conditions, like accepting cooling water temperature up to 35°C and removing the need for an external chiller. The camera is fully sealed, includes the Thermo Electric Cooler controller inside the camera head, and needs only a standard +24V power supply for the whole system.

The OCAM2 system is capable of driving all members of the CCD220/219 family at their nominal speed (1.5kframes/s) and transmitting the data at full speed through a CameraLink interface. The camera controller is able to drive deep depleted variants with multilevel clocking at voltage levels up to 24V with speeds of 10Mlines/s (at a nominal phase load of 1nF). To obtain such a speed, OCAM2 uses a special phase generation scheme. An arbitrary waveform generator is used. The core sequencer feeds a fast 14bit D/A converter running at 109 Mfps followed by a class AB power amplifier that drives the CCD's phase. Using this generation method, it is possible to compensate for the parasitic PCB track/package pin inductance that makes a resonator with the CCD's phase and produce potentially destructive overshoots by using de-emphasis and suitable drive waveforms. This method can also be used to reduce the slew rate of the phase drive in order to minimize the generated Clock Induced Charges (CIC) [17].

The controller handles the 8 L3vision outputs with high voltage clocking up to 50V voltage swing. A big effort has been made to have high voltage stability (less that 1mV/hour of drift) in order to ensure a constant gain over a long period. The system digitizes the CCD signal using correlated double sampling with 14 bits resolution. Standard interfacing of the camera is performed by using a PC computer running Windows OS fitted with a CameraLink full grabber and a proprietary software capable of gathering in real time the extremely high data rate of 220Mbytes/s produced by the camera.

In addition, the team developed a user-friendly timer file editor to manage the clock sequencer of OCam. The sequencer itself is the heart of the system; it has a nominal resolution of 1.5ns and is capable of generating clocks at a frequency of 327MHz. The phase jitter was measured at a level of 60ps RMS.

1.4 OCAM2 and CCD220 performances

Camera presentation

The OCAM2 camera is shown in Figure 3 and a screenshot of the data acquisition GUI used for camera optimization and characterization is shown in Figure 4.

Figure 3: OCAM2 camera pictures. (left) back side of the camera; (right) front side of the camera.

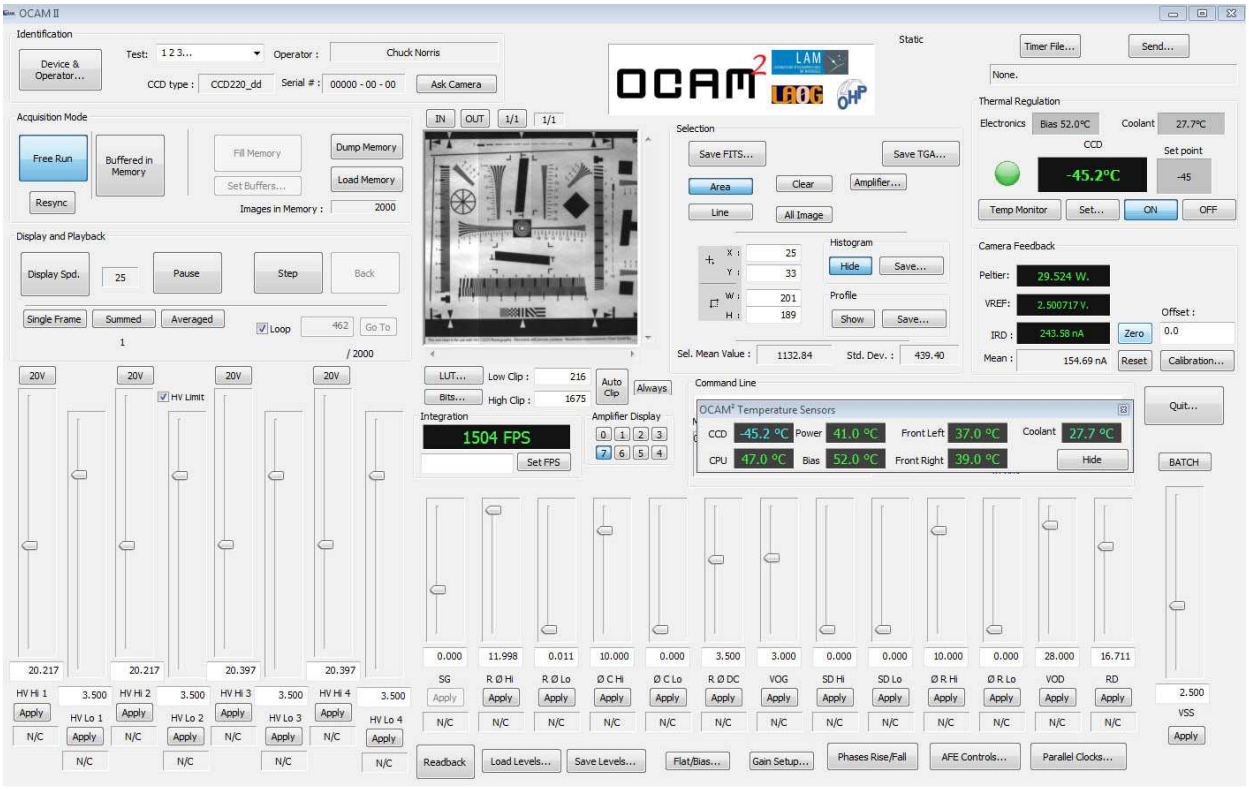

Figure 4: screenshot of the OCAM2 GUI used for camera characterization showing image acquired at 1504 fps with detector cooled at -45°C.

Testing procedure

The 8 outputs of OCAM2 are numbered using the following labels order inside the image:

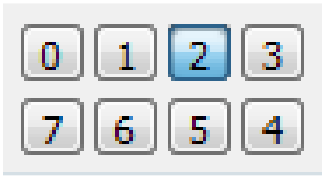

System gain

The system gain, in adu/e, gives the conversion between adu stored in the FITS image files and the number of electrons integrated in the pixel.

The system gain is deduced from the Reset Drain Current (IRD), in Amps (A), measured in each frame by a high precision ammeter. The detector is illuminated by a flat field provided by an integrating sphere.

The IRD current is first converted in signal S (e/pixel/frame) using the following formula:

$$S = \frac{IRD}{e.F} (Eq. 1)$$

Where F is the Frame Rate (in fps)

And e is the electron charge (in C).

Then for several illumination levels, the signal S is plotted as a function of the mean signal.

The slope of this curve gives directly the system gain in e/adu.

Multiplication gain, dark and Noise with gain

The standard way that dark current and the multiplication gain is determined for each output is based on an e2v technical note for estimating ultra low level of dark signal in EMCCD devices [20]. If the majority of dark signal is generated in the image/store section, then the dark signal level can be extracted from a simple analysis of the output distribution, even at very low signal levels.

For a certain threshold T of the pixel value, $N_d(T)$ is the fraction of pixels of the distribution that are above the threshold T, G is the multiplication gain and S_{dark} is the dark signal. $N_d(T)$, T, S_{dark} and G are linked by the following equation:

$$Ln(N_d(T)) = Ln(S_{dark}) - T/G \quad (Eq.2)$$

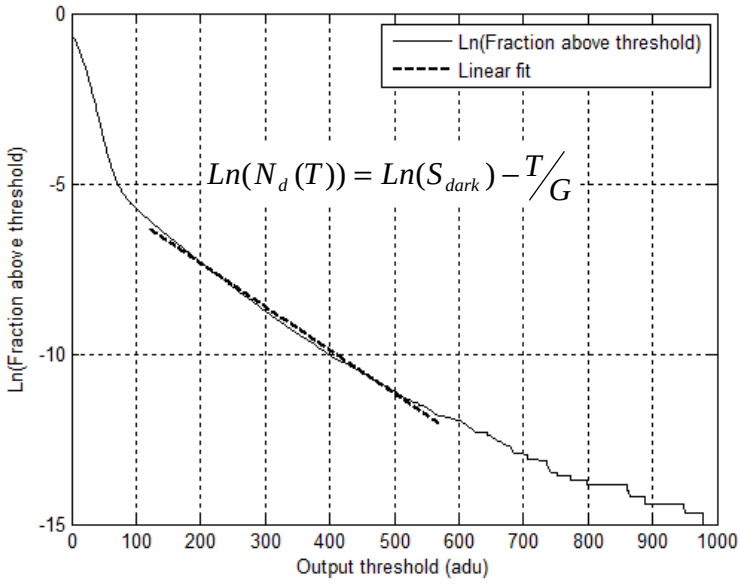

Figure 5. Method for computing dark signal and multiplication gain on the EMCCD when the camera is operated with multiplication gain [19]. Statistics are obtained by combining all the pixels of a single output over 2000 consecutive frames (60x120 pixels, 2000 dark images). N_d is the fraction of pixels that are above a given threshold T, S_{dark} is the dark signal and G the multiplication gain. The dark signal and the multiplication gain is determined by fitting a straight line to the linear part of this figure.

This equation is only valid if the chance of getting two electrons in a pixel is insignificant. When this equation is valid, the plot of $Ln(N_d(T))$ as a function of the dark signal S_{dark} is linear. Measuring the slope of this linear plot and the intercept with the vertical axis, the dark signal S_{dark} and the multiplication gain G can be computed. The Figure 5 shows a typical plot. The linear part of the plot is fitted in order to derive the dark signal and the multiplication gain. The plot is obtained by combining the 60x120 pixels of an output of 2000 consecutive dark images acquired at 1500 fps. The test is performed in complete darkness, thus reducing the possibility of damaging the CCD.

To compute the noise with multiplication gain on the CCD, a set of 2000 consecutive dark images is recorded with multiplication gain (~ 42-43V on high voltage clock).Then for each output, the histogram of all the 60x120 pixels over the 2000 images is plotted to have good statistics. The mean signal is subtracted to obtain centered histogram. RMS noise is computed by fitting the histogram with a Gaussian equation:

$$N(x) = A.e^{-x^2/2\sigma^2} \quad (Eq.3)$$

where σ is the measurement of the camera readout noise (in ADU).

The Figure 6 shows a typical noise histogram with multiplication gain (here 1500). Also shown on this figure is the Gaussian fit of the histogram:

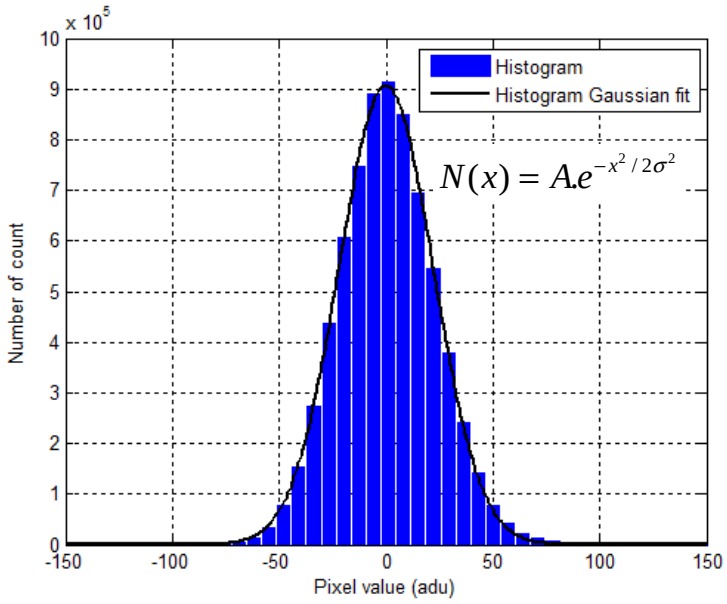

Figure 6. Method for computing readout noise with multiplication gain on the EMCCD. The signal is measured here includes the multiplication gain of the EMCCD (multiplication gain is here 1500). The σ parameter of the histogram Gaussian fit is the RMS noise of the camera.

From the Gaussian fit of the histogram, the RMS readout noise can be derived which is equal to the σ fitted value.

Estimating low multiplication gain <400: the "direct" method.

The previous method does not allow to estimate multiplication gain below x400, and the accuracy of the method decreases with the number of events, i.e. the multiplication gain.

Therefore a direct method measurement is also used.

The CCD is illuminated with a flat image of very small level, close to 20 adu.

The stability of the bias level needs to be very good by running the camera at least 1 hr before taking data. Same consideration for the integrating sphere illumination, this one has to be started a long time before measurement to be extremely stable. Then the level value is estimated from a small window where the signal is completely flat with an excellent accuracy by averaging 2000 consecutive images (bias image is subtracted). Then, the gain is applied by increasing the HV voltage, and the same window with 2000 image average is used to estimate the level of the image with multiplication.

Dividing the mean level of the multiplied image by the mean level of the image at gain 1 gives a direct measurement of the multiplication gain (in each case after subtraction of the mean bias image).

This method can be used until the multiplication register is saturated.

1.5 Tests results

For all tests reported here, the camera is operated at 1503 fps in a dark room, the CCD220 is cooled at -45°C.

Multiplication gain calibration

Using the "direct gain measurement " method described in section 1.4, the multiplication gain has been calibrated for each output as show in Figure 7. The Figure 8 shows how the previous plot is inverted and used as calibration for the camera. The entry of the table is the gain, the output is the High Voltage (HV) phase used by the camera.

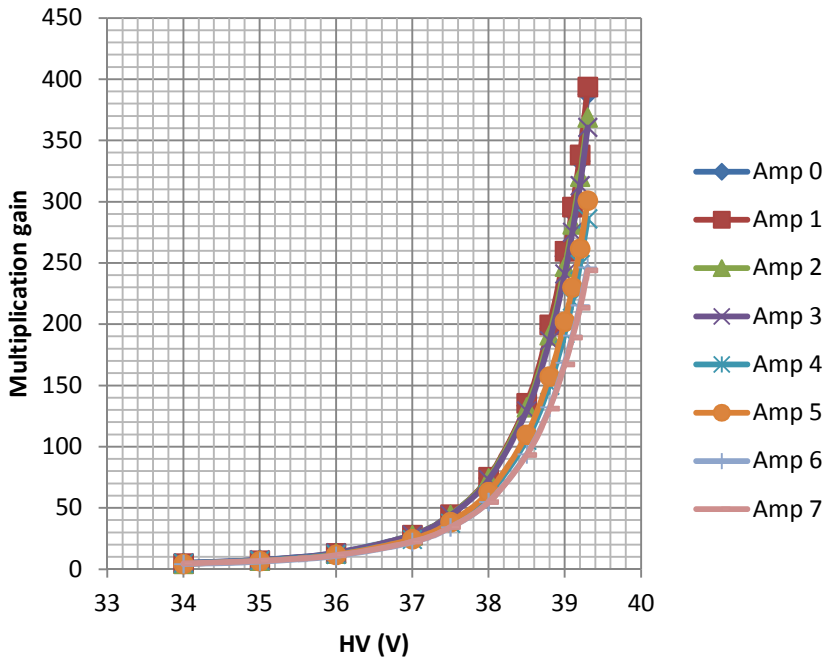

Figure 7: multiplication gain calibration at a temperature of -45°C as a function of HV voltage for a standard silicon CCD.

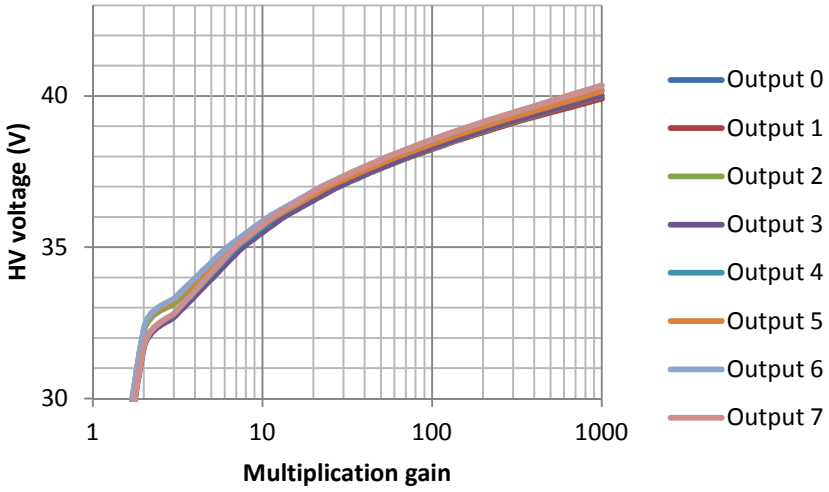

Figure 8: inversion of previous plot at a temperature of -45°C: HV voltage function of gain for a standard silicon CCD.

To verify the camera calibration, the multiplication gain is set to x300 using the OCAM GUI. Then the multiplication gain is measured for each output using the direct gain measurement method showing an excellent agreement between the set value and the measured gain, see Table 1.

Output	Gain
0	299.7
1	300.0
2	304.9
3	290.2
4	290.1
5	301.7
6	300.8
7	297.3

Table 1: gain measurement for a x300 gain setup at a temperature of -45°C.

Image example with multiplication gain x150 after gain calibration

To demonstrate the image quality with gain and give an example of the S/N improvement with gain, an image has been recorded with low flux conditions. Then the multiplication gain has been increased to x150. The S/N improvement can clearly be seen on the image, see Figure 9.

We can note that the multiplication gain of each output is perfectly matched so that the 8 outputs of the CCD can not be distinguished on this image, as if there was only one output (see Figure 9).

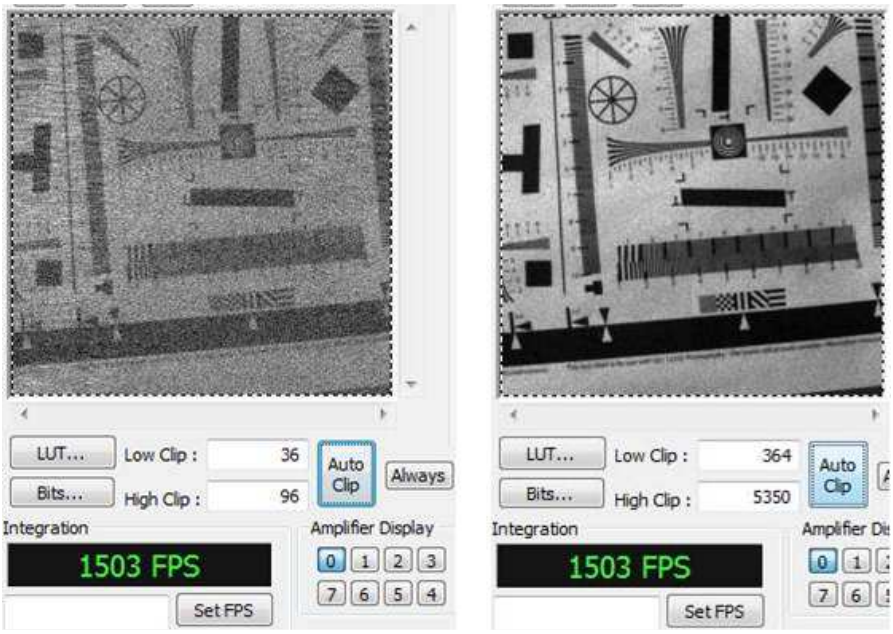

Figure 9: left: image recorded under low flux condition, mean image is about 40 adu. Right: the same image with a gain x150. Detector is at -45°C, frame rate is 1503 Hz. Perfect multiplication gain matching can clearly be seen on this image.

Dark measurement at multiplication gain x600

The camera is operated at 1.5 kHz in the dark, the CCD is cooled at -45°C. The Dark current is measured using the Eq. 2.

With a multiplication gain of x600 and a frame rate of 1.5 kHz, the measured dark is given in Table 2.

Output	Dark (e/pixel/frame)
0	0.0240
1	0.0011
2	0.0007
3	0.0020
4	0.0015
5	0.0013
6	0.0021
7	0.0024
Mean	0.0044

Table 2: for 1.5 kHz frame rate, at a temperature of -45°C, this table gives the measured dark signal.

Fix Pattern Noise (FPN)

From dark images at gain x1 and x600, the fix pattern noise (FPN) of each output is computed. The FPN input referred is the FPN divided by the multiplication gain. The FPN results are given in Table 3 (left: gain x1; right: gain x600). The FPN input refereed is the FPN divided by the multiplication gain. The FPN is of the same order of magnitude as the readout noise.

Output	FPN (adu)	FPN (e-)	FPN input (e-)
0	17.0	281	281
1	11.0	182	182
2	9.6	159	159
3	14.1	233	233
4	7.4	123	123
5	5.6	92	92
6	6.8	112	112
7	12.8	211	211

Output	FPN (adu)	FPN (e-)	FPN input (e-)
0	19.2	317	0.53
1	10.6	174	0.29
2	8.9	147	0.24
3	13.6	224	0.37
4	7.9	130	0.22
5	5.4	89	0.15
6	6.6	110	0.18
7	11.1	184	0.31

Table 3: (left) FPN at Gain x1 and 1500 fps; (right) FPN at Gain x600 and 1500 fps.

Typical OCAM2 readout noise performances

The Table 4 shows the typical readout noise performances of the OCAM2 camera, the example shown hereafter is the readout noise measured of the camera delivered to ONERA. The typical readout noise variation with gain is shown in the Figure 10. This curve is measured for a frame rate of 1503 fps and a detector temperature of -45°C. This plot shows that a mean readout noise of 0.5e can be achieved at a modest multiplication gain of x200.

Gain	1	200	600
Output 0	98	154	157
Output 1	82	84	85
Output 2	72	73	73
Output 3	115	122	124
Output 4	74	107	109
Output 5	75	74	75
Output 6	79	77	77
Output 7	86	80	80
Mean	85	97	98

Gain	1	200	600
Output 0	98	0.77	0.26
Output 1	82	0.42	0.14
Output 2	72	0.36	0.12
Output 3	115	0.61	0.21
Output 4	74	0.54	0.18
Output 5	75	0.37	0.12
Output 6	79	0.39	0.13
Output 7	86	0.40	0.13
Mean	85	0.48	0.16

Table 4: (left) OCAM2 noise for gain x1, x200 and x600, at the output; (right) OCAM2 noise for gain x1, x200 and x600 input referred (previous noise divided by gain). Detector temperature is -45°C.

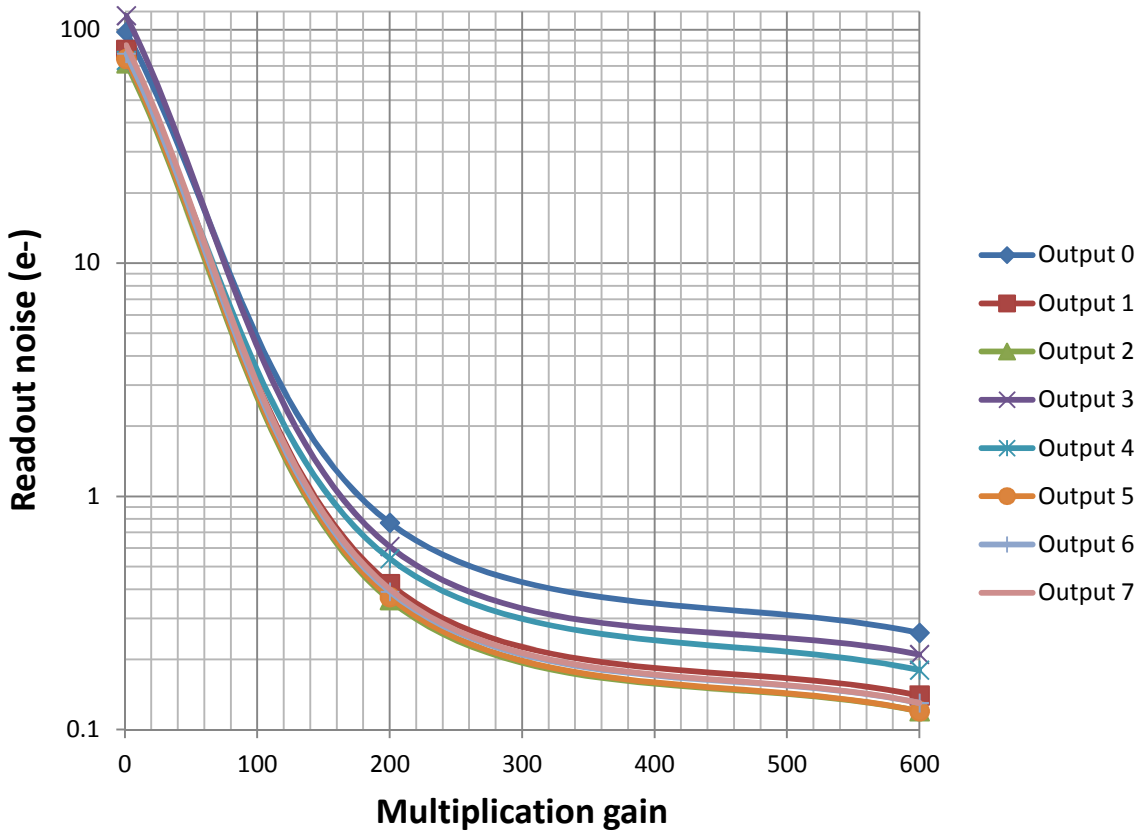

Figure 10: typical OCAM2 readout noise as a function of the multiplication gain at 1503 fps. Detector temperature is -45°C. Mean readout noise of 0.5 e can be achieved at a modest multiplication gain of x200.

Frame rate measurement

An optional board inside OCAM2 can be added to drive a frame synchronization signal on a physical connector located on the back side of the camera. This signal can be used to synchronize a system with OCAM2. The frequency of this signal is the frame rate. A frequency counter with 10 digit accuracy has been used to directly measure the frame rate demonstrating a real operation of the camera running at 1503 fps.

Figure 11: a frame rate of 1503.288 Hz has been measured using the frame synchronization signal, the frequency counter is shown on this picture.

Quantum efficiency

The Quantum Efficiency (QE) of the detector is also a major parameter of the system sensitivity. The QE of the Standard Silicon and Deep Depletion CCD220 was measured and typical results are shown in Figure 12.

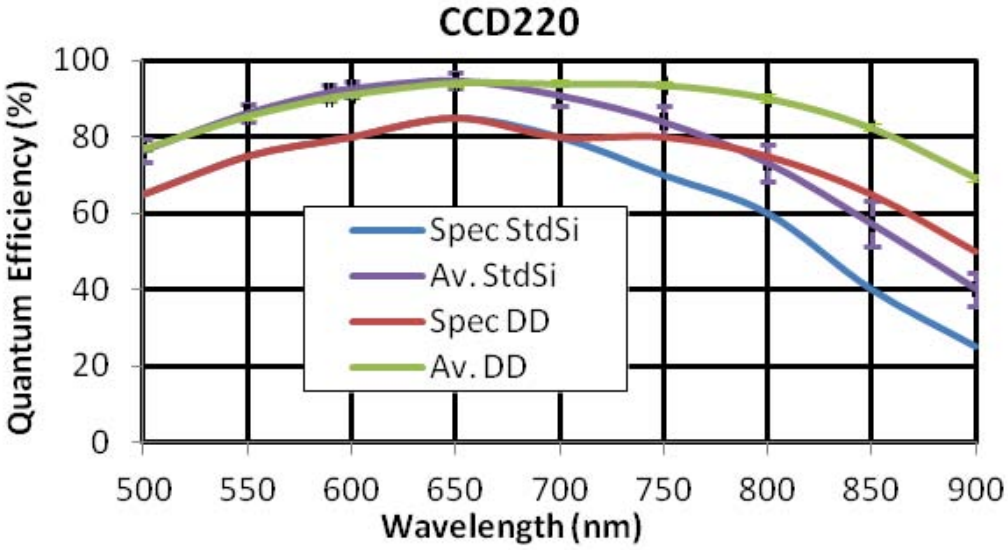

Figure 12. Measured average QE (e2v) of 16 Science Grade Standard Silicon (labeled StdSi) and 4 Deep Depletion Silicon (labeled DD) CCD220s compared to the contract specification. All are > 5% higher than the specifications. The > 20% higher QE in the "red" illustrate why the Deep Depletion are highly sought after for NGS applications, from [22].

Additional features

Whereas OCam has been designed to test CCDs and to have a lot of tuning capabilities (voltages, features and so-on), OCAM2 is a ready-to-use camera with embedded parameters to run the CCD, factory optimized. Apart from this, OCAM2 has been designed to be ruggedized and can accept more demanding environmental conditions, like a cooling water temperature up to 40°C making unnecessary a secondary external chiller. The camera is fully sealed, includes the

Thermo Electric Cooler controller inside the camera head, and needs only a standard +24V power supply for the whole system. The OCAM2 camera is now a commercial product of First Light Imaging [19]. First Light Imaging also designed and fabricated the front end analog board of the ESO wavefront sensor camera fully described in [21].

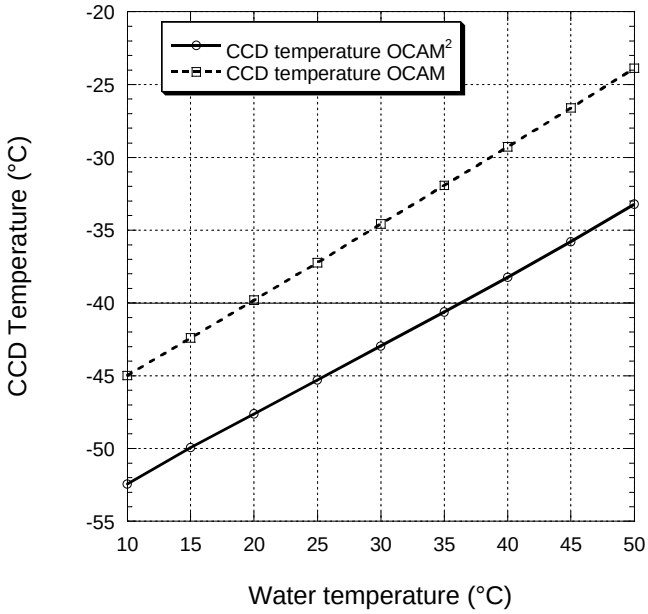

Figure 13. CCD temperature as a function of water temperature (flow of 1.5 l/min) used in the heat sink dedicated to cool down the Peltier hot side with outside air temperature of 30°C. As shown on this figure, OCam^2 can accommodate a water temperature as high as +40°C with a CCD temperature close to -40°C in these rugged conditions.

OCAM2 uses high performance FPGAs and can do instant on-the-fly pre-processing like dark / bias subtraction and flat-gain correction lowering the real time computer power that is required. OCAM2 provides not only an industry-standard CameraLink full interface but also duplex serial protocols over multimode or monomode optic fibers using standard SFP modules. Protocols like PCI Express, RapidIO and Infiniband are supported. Other specific or even proprietary fiber links can be implemented upon special request. Unique external synchronization and clock inputs of OCAM2 ensure a perfect synchronous operation of any number of OCAM2 at the nanosecond level. It is possible to synchronize OCAM2 with any external device (pulsed laser, another OCAM2 camera, master timer) with a precision of 10ns. OCAM2 includes also a modified mechanical design allowing integration of any type of microlens array for use of this camera in all kind of wavefront sensing AO applications. The front cover of OCAM2 can be easily modified to include a microlens exchange mechanism. The size of the camera head is extremely compact with a 238.5x175x76.2 mm footprint that includes all electronics, the CCD and the cooling system embedded in a robust aluminum sealed cover. The services needed to operate the camera are not demanding. OCAM2 only needs a 24V DC power supply and a water cooling system with the following typical specifications: a water flow of 1.5 l/min, a cooling power of 50W, and water temperature between 10 and 35°C.

With the capability of running at 2-2.5 kfps by using optimized clocking, a special preamplifier design that rejects clock feedthrough, and many other features, OCAM2 makes it an interesting contender for AO applications of the planned generation of Large Telescopes instruments.

OCAM2 in the ONERA AO bench: real AO demonstration at 1503 fps

Since the beginning of 2012, a specific collaboration between First Light Imaging [19], ONERA and SHAKTI has been initiated for integrating the OCAM2 camera in the ONERA AO bench (BOA) specifically design to run at very high temporal frequencies (up to 2 kHz). This collaboration as several objectives:

1) Integration and tests of OCAM2 in a dedicated AO bench, see Figure 14, especially designed at ONERA for high performance at visible wavelengths. The bench is composed by a 10x10 CILAS DM (piezo-stack technology) used in a 9x9 actuator configuration, a dedicated fast tip-tilt mirror (PI component), a Linux based RTC (ORCA) optimized for high speed operation although extremely versatile (allowing to deal with SCAO, MCAO and LTAO systems all tested at ONERA). Several auxiliary loops (pupil stabilization, pupil derotation, non-common path aberration compensation) have also been implemented in order to ensure an efficient operation and a good performance on sky.

Figure 14: the OCAM2 camera integrated in the ONERA AO bench.

2) Coupling OCAM2 with the ORCA RTC (developed in the FP7-OPTICON JRA1framework). ORCA is an Open RTC Architecture (developed by SHAKTI Cie) allowing outstanding performance with simple LINUX based PC. This aspect will be fully achieved in two successive steps. Firstly a simple coupling will be done without fully optimizing the computation of Shack-Hartman measurement while CCD readout. This allows us to have very decent performance although the loop delay (from the end of the CCD integration to the voltage application) remains quite large, typically around 2 – 2.5 frames. This first step has been achieved and a AO loop bandwidth (defined at 0dB of the rejection transfer function) larger than 70 Hz (1500 Hz of sampling frequency and 2.5 frames of loop delay) has been already measured in lab as shown in Figure 15.

   The second step (currently under development) consists in optimizing the Centre of Gravity (CoG) measurement by taking benefit from the multi readout of the OCAM CCD (8 outputs). CoG measurements will begin as soon as a first bunch of pixels (typically a few lines per outputs) will be read. This will lead to dramatically reduce the overall loop delay down to typically 1.5 frames and thus increase the AO bandwidth up to 100 Hz.

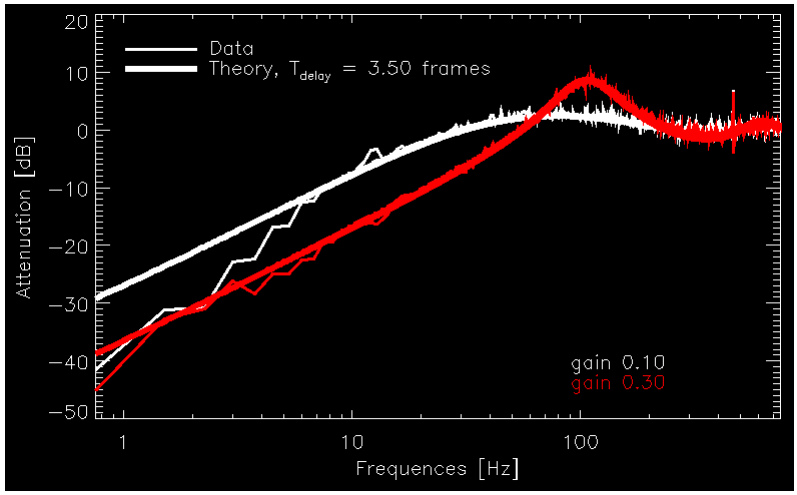

Figure 15 Rejection transfer function of the AO loop system. Sampling frequency is 1503 Hz (accurately measured at the output of the OCAM camera). All RTC processes (CoG measurements, voltages computation, temporal filtering) are performed in less than 1 ms. The Total delay is then 1 frame of integration (666 µs), 1 frame of transfer (666 µs) and 1.5 frames of RTC computation (1 ms). The measured AO loop bandwidth is 70 Hz.

3) On-sky tests of the AO bench on a 1.5m telescope at Observatoire de la Cote d'Azur. At least two runs of on sky tests are foreseen during summer and fall 2012. The first run (which will last at least 10 days) will be dedicated to the coupling of the AO bench and the telescope and to the very first tests and performance. The second one will be fully dedicated to fine characterization and extensive performance assessment of the system.

After the two first runs, the AO system will permanently stay on the telescope. The WFS path of the system has been specifically design to include simultaneously 2 WFS in order to perform on sky comparison of new concepts. At least two experiments are already foreseen with this unique tool in the next future: the development of a Pyramid WFS with OCAM2 (direct on sky comparison of Pyramid and SH-WFS) and the development of an IR WFS based on the RAPID concept (see Section 3) and comparison between VIS and IR WFS with state-of-the-art components.

E2v CCD220 and OCAM2 performances measurement summary

Many other features of the CCD220 were tested with conventional methods that are not described here. The OCAM2 and CCD220 measured main performances are summarized in Table 5.

Test measurement	Result	Unit
Mean readout noise at 1300 fps and multiplication gain ~ x600	<0.2	e
Dark signal at 1300 fps at -40°C	< 0.01	e/pix/frame
Dark signal at 25 fps at -40°C	< 0.05	e/pix/frame
Detector operating temperature	-40	°C
Peak Quantum Efficiency at 650 nm	94	%
Linearity at gain x1000 from 10 to 150 ke	<3	%
Image area Full Well Capacity at gain x1, 1300 fps	300000	e-
Parallel CTE at gain x1, 1300 fps	>0.99995	N/A
Serial CTE at gain x1, 1300 fps	0.99994	N/A
Maximum Deviation from Peak to Valley over the light sensitive area	0.7	µm
Optical Distance from CCD image plane to front of window	3.33	mm
Angle between CCD image plane and front of window	<0.2	degrees

Table 5. e2v CCD220 (standard Si) and OCAM2 measured performance summary.

2. THE NGSD: A 880X840 700 HZ 3E CMOS DEVICE FOR NATURAL/LASER GUIDE STAR WAVEFRONT SENSING ON ELT

2.1 Introduction: a CMOS AO detector roadmap for E-ELT.

A new fast detector development in the visible has been started by ESO and the OPTICON network in 2008 to develop new detector devices in the E-ELT framework, both for NGS and LGS wavefront sensing on extremely large telescopes. The same consortium with ESO, e2v technologies and the French astronomical observatories (LAM, IPAG and OHP) decided to develop a long term program for this goal with joint funding from ESO and OPTICON under the 7th Framework Programme.

Very early in the project, it has been decided to move to new detector technologies based on CMOS devices. But if CMOS devices are now commonly used in low cost applications, this is not the case for demanding scientific imaging. To mitigate the risk of this technological step, the long term programme was divided into several phases, up to the LGSD (Laser Guide Star Detector) which is the final development. The different phases are "Technology Demonstrators" (TVP), see Figure 17, the "Natural Guide Star Detector" (NGSD) and the LGSD. The timescale of this programme is shown in Figure 18. The main issue with Laser Guide Star wavefront sensing is the spot elongation due to the finite distance of the laser guide star produced by the stimulation of the sodium layer of the atmosphere at about 90 km, see Figure 16. This cone effect due to the angle between the telescope axis and the laser beam axis induces that LGS spots are elongated as shown in the Figure 16. The main consequence is that the LGS sub-aperture requires more pixels than with NGS whereas all other parameters of the AO detector remain the same: frame rate, pixel size, quantum efficiency, dark current and up to a certain level the readout noise. Maintaining fast frame rate (~ 1 kHz) and low readout noise lower than 3 e while increasing the detector format is impossible with the current detector technology. This is the reason why a new devices family is under development to cover this new exciting challenge for the E-ELT.

Simulations showed that the NGSD and LGSD ideal format would be:

- For the Natural Guide Star Detector (NGSD): 84x84 sub-apertures of 8x8 pixels
- For the Laser Guide Star Detector (LGSD): 84x84 sub-apertures of 20x20 pixels

An early plan was to design a Scaled Down Demonstrator (SDD), see Figure 17, a reduced size version of the final Laser Guide Star Detector (LGSD), as a significant step towards the full size imager. This was a proof of concept and of performance. The SDD has now been superseded by the NGSD, still a small version of the LGSD, but with a minimum size to allow use of smaller subapertures (8 × 8 pixels) in a full size array (84 × 84) of sub-apertures. This allows an ELT to use natural stars in its AO system. The same array can be read in 20 × 20 pixel sub-apertures for use with laser stars in the AO system in a smaller telescope. The NGSD is designed in blocks that can be repeated to assemble a full LGSD with the minimum of re-design (detector stitching).

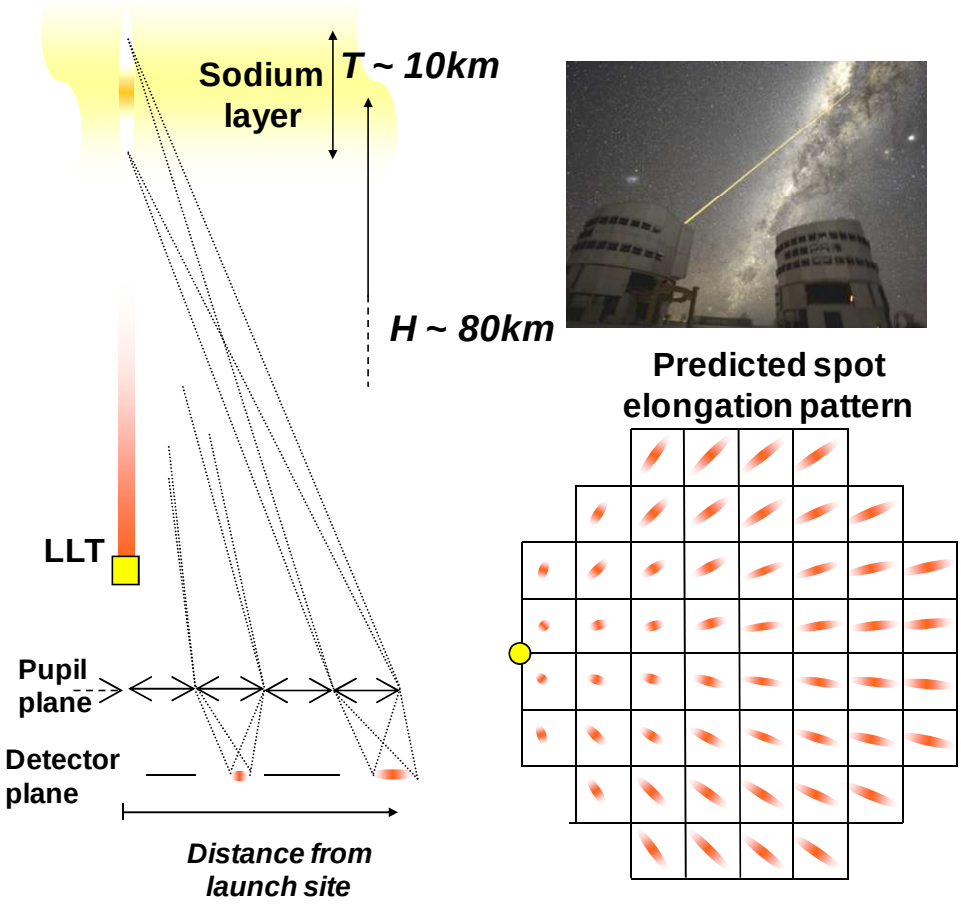

Figure 16: the spot elongation issue with Laser Guide Star wavefront sensors

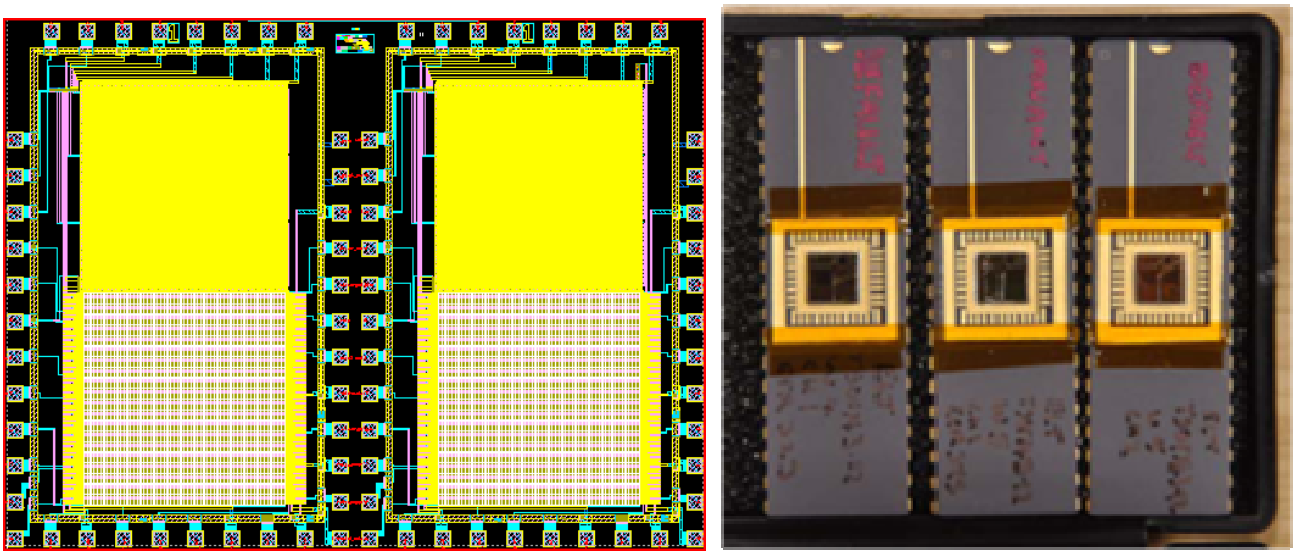

Figure 17: CMOS Technology Demonstrator for the NGSD: (left) Technology Demonstrator layout; (right) picture of the devices tested.

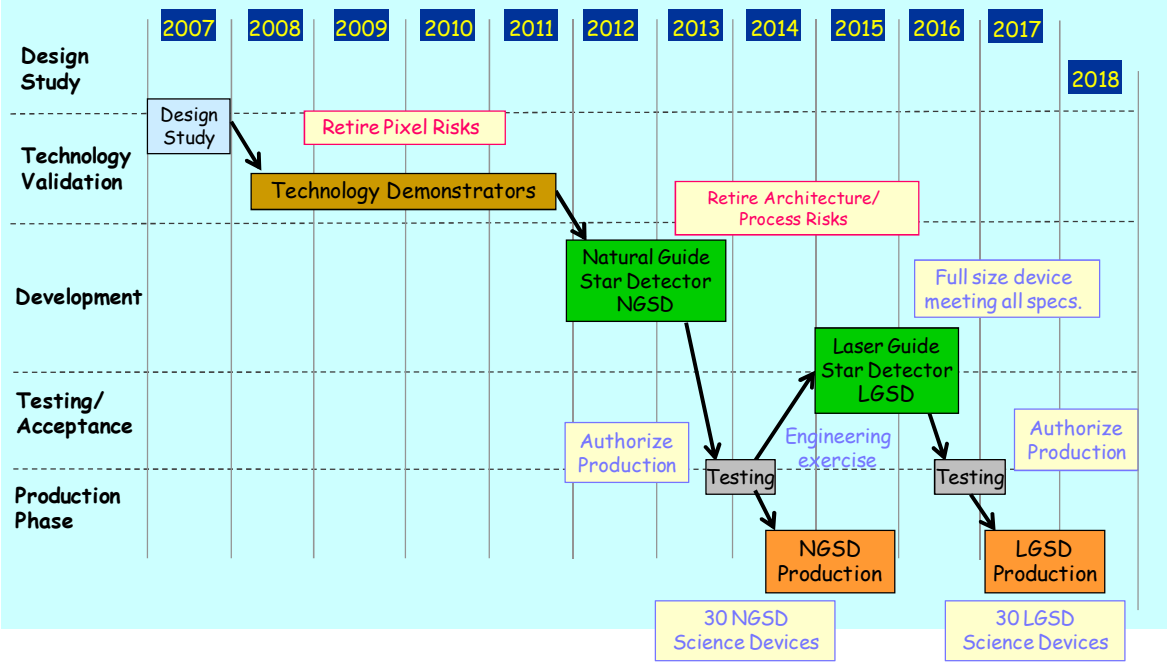

Figure 18: The multi-phase development plan of the large optical NGS/LGS WFS detector showing how risk is progressively retired; Design Study to investigate possible technologies, Technology Demonstrator to retire pixel risks, ¼ full size Scaled Down Demonstrator (NGSD) to retire architectural and process risks and to ensure devices are available on time for first light E-ELT instruments, the full scale development (LGSD) which should be mostly an engineering exercise, and finally production run to manufacture 30-50 devices.

2.2 The e2v NGSD CMOS detector presentation

A extensive description of this device development can be found in [22] with a full presentation of the detector design and trade-offs. Hereafter are only summarized the main characteristics of the laser guide star CMOS detector. The purpose of the NGSD was twofold: a) to retire architecture and process risks without the high costs of stitching (required for the final device) or custom Peltier packages; i.e. to be a low cost (relatively) scaled-down demonstrator, and b) to be large enough (> 672x672 pixels) to be able to be used as a detector for first light AO systems on the E-ELT (requiring 10x10 pixels per sub-aperture and 60x60 sub-apertures). The NGSD (see Figure 19 for comparison of NGSD and LGSD) is designed to meet all requirements of the final full size device, the LGSD, except for the pixel format size.

The rapid progress has come about through several innovative improvements [23] : a) Pinned Photo Diode (PPD) that substantially reduce the dark current, b) high conversion gain (by reducing the sense node capacitance) that amplifies the signal above the noise and obtains effective low read noise of under 3e-, c) buried channel MOSFETs that reduce/eliminate random telegraph signal (RTS) noise and background flicker noise associated with the surface states in the source follower pixel and reset amplifiers, d) improvement in QE and pixel crosstalk of the CMOS imager by back-side illumination and building the sensor from thicker high resistivity silicon (> 10,000 ohm-cm), and high voltage 'substrate biasing' to efficiently collect charges generated deep within the silicon, without pixel crosstalk and consequential blurring, and to extend the wavelength response into the near red.

Conceptual block of the LGSD (BSI CMOS Imager), see Figure 19, consists of a 1760 x 1680 square grid array of pixels addressed from either side and read out from both top and bottom. The central 1680x1680 pixels will be light sensitive while the outer 40 columns either side will be optically masked and used as reference pixels if required. Many rows of pixels are read in parallel to allow enough processing time per pixel to beat down the noise and the ADCs to digitize the signal. The data is multiplexed and transferred off-chip through a fast LVDS serial digital interface. The Table 6 summarizes the main NGSD and LGSD characteristics.

Table 6: the e2v NGSD and LGSD CMOS device main characteristics

Pixel number (including dark reference pixels)	"Natural Guide Star Detector" NGSD - 880x840 pixels with 840x840 sensitive pixels "Laser Guide Star Detector" LGSD - 1760x1680 pixels
Detector technology	Thinned backside illuminated CMOS 0.18µm
Pixel Pitch	24µm
Pixel topology	4T pinned photodiode pixel
Sub-aperture	20x20 pixels
Array architecture	NGSD: 42x42 sub-apertures of 20x20 pixels LGSD: 84x84 sub-apertures of 20x20 pixels
Shutter	Rolling shutter in chunks of 20 rows → synchronous detection within a sub-array.
Responsivity	100 to 160 µV/electron
Pixel full well	4000 e-
Read noise including ADC	< 3.0 e^-_{RMS}
ADCs configuration	NGSD: 20 x 880 column ADCs, 9 (goal 10) bits LGSD: 80 x 880 column ADCs, 9 (goal 10) bits
Number of parallel LVDS channels	NGSD: 22 LGSD: 88
Serial LVDS channel bit rate	210 Mb/s baseline, up to 420 Mb/s (desired)
Frame rate	700 fps up to 1000 fps with degraded performance for both LGSD and NGSD
Detector power dissipation	Specification: maximum 5W , including the LVDS drivers

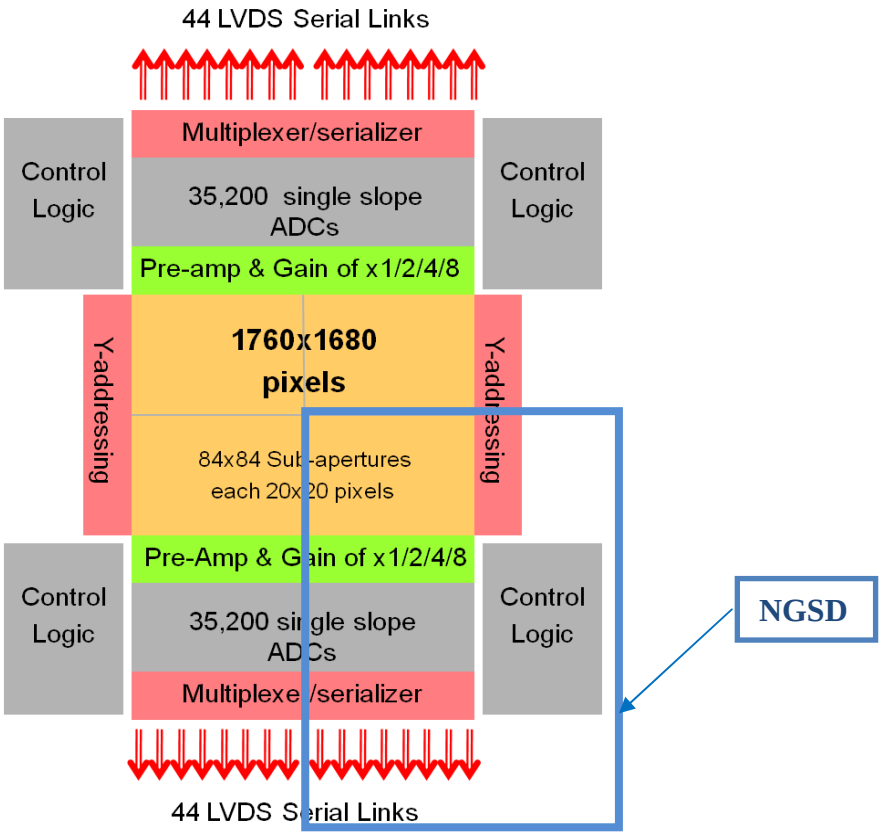

Figure 19: the e2v LGSD and NGSD CMOS detector block diagram

The LGSD will be ~ 45mm x 50mm in size and thus will require stitching. The NGSD will not need to be stitched, and thus, is designed to fit within a single reticle of 25.5mm x 32.5mm. However, the NGSD is designed with stitching in mind (in order to be a true demonstrator), and will follow the stitching plan of Figure 20.

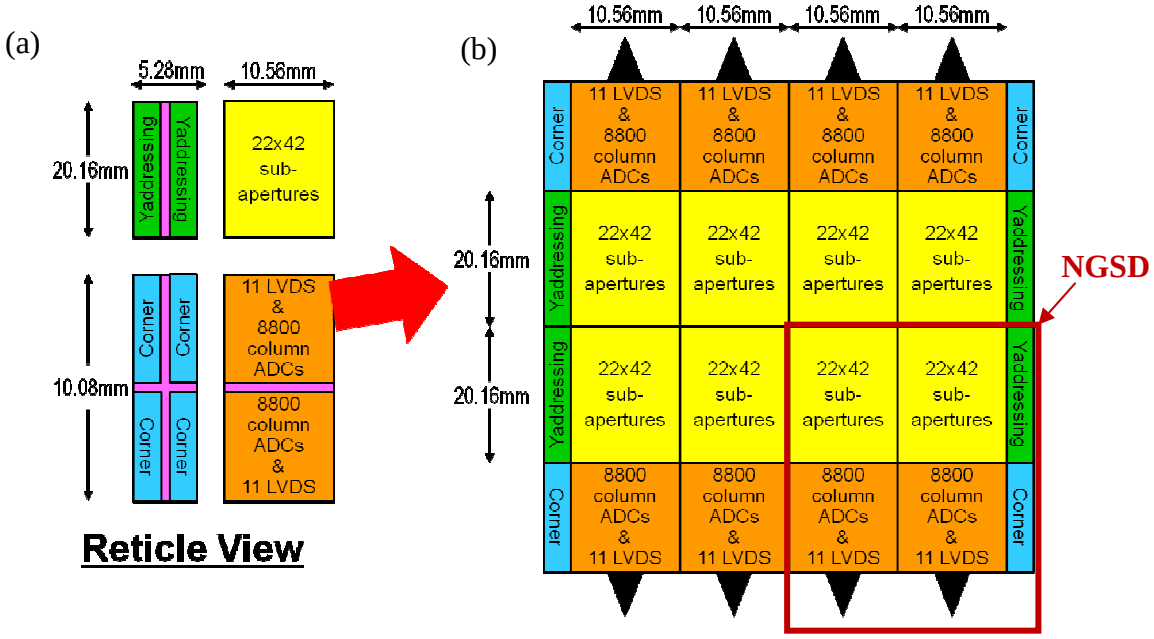

Figure 20: The LGSD stitching plan: a) The four reticles from which the whole device on the right can be manufactured, b) Stitching layout of LGSD. NGSD is shown in red. Note that the NGSD is not be stitched.

2.3 The NGSD CMOS Camera system development

The camera controller is a key system and a challenging device since it has to handle a very high throughput (in the range of 40Gb/s for the LGSD). Thanks to highly parallelized architecture of FPGAs, initial data rate is pretty easy to handle but data transfer from controller to RTC at required rate and minimal latency is the key issue for this design. This is a well known problem: connectivity and latency are major issues in datacenters and intensive computing. The camera controller will use then the same solutions with Infiniband & 10/40/100 GigE transmission path. The camera will then require only a power supply, a duplex fiber and some cooling water circuit to provide images. The expected latency of the transmission line to the RTC is in the range of 7.5 µs and the used configuration will be linearly scalable in order to be compatible either with the NGSD device or the LGSD device. It is also requested to include on-the-fly pre-processing (bias subtraction and flat correction) without any significant latency. This has been already successfully demonstrated on an OCAM2 camera which provides this as a standard feature now, with a scalability to NGSD and LGSD devices.

The controller breakdown structure is shown in the Figure 21. A preliminary design of the camera head with its cooling system and readout electronics is shown in the Figure 22 demonstrating compact overall dimensions as small as 100 x 130 x 112 mm^3.

A camera system, fabricated by First Light Imaging [19], using the e2v NGSD device will be a commercial product offered to the astronomical community by 2014.

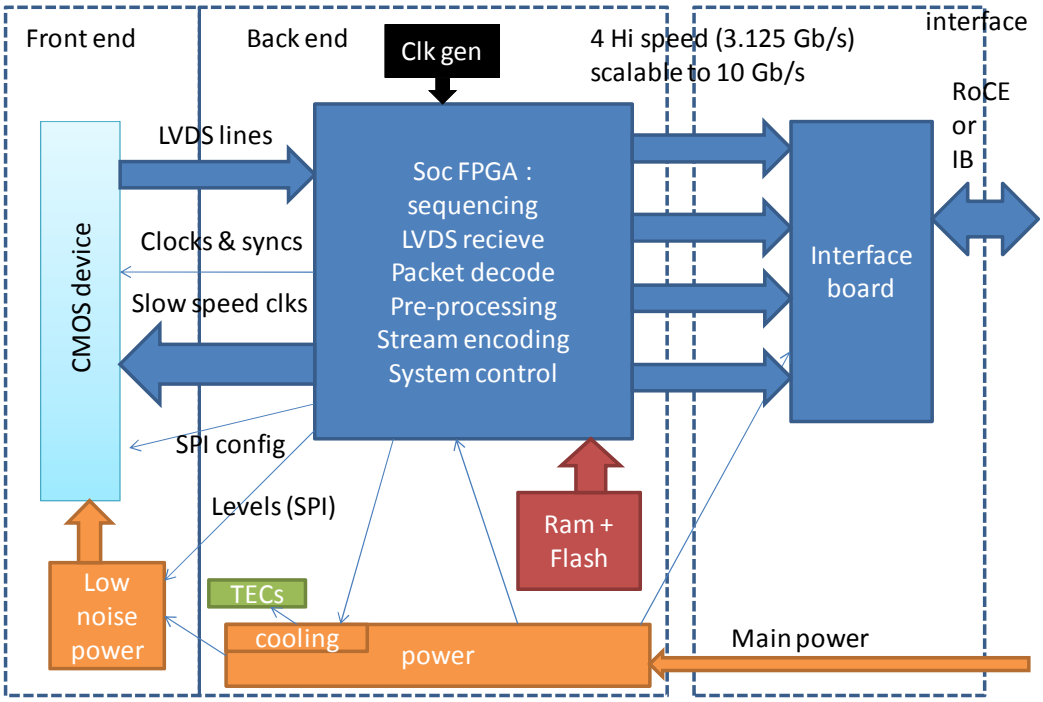

Figure 21: schematic of the camera controller for the NGSD

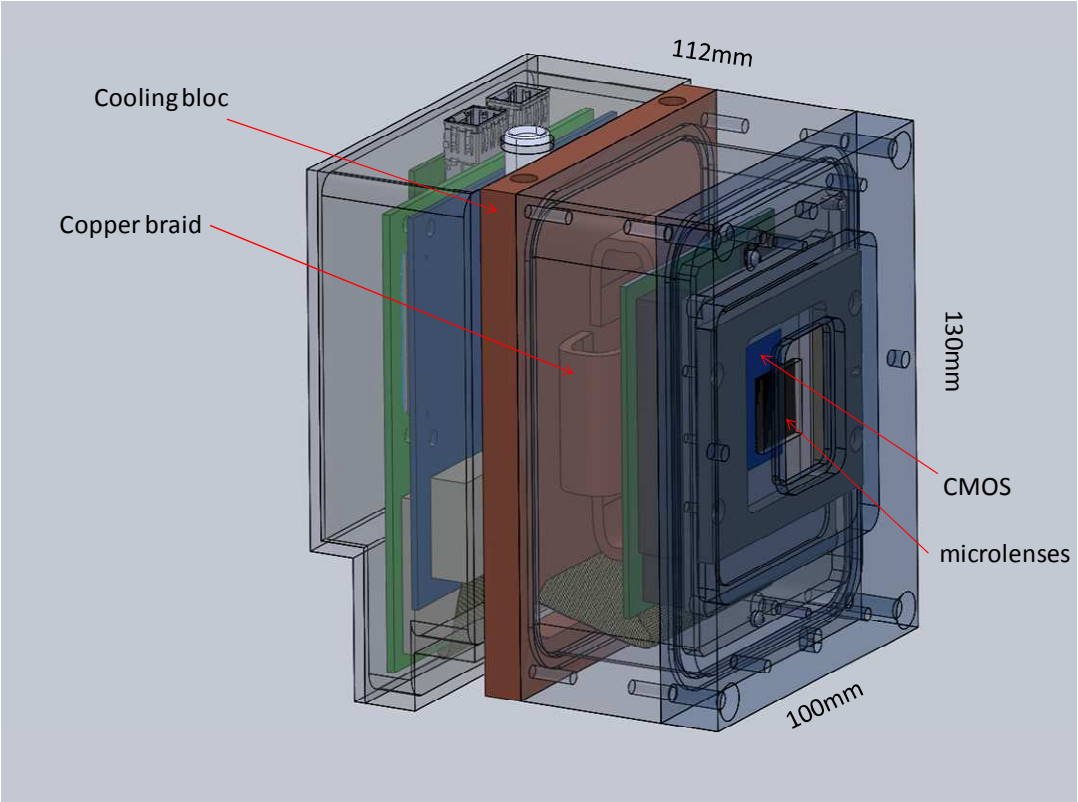

Figure 22: the NGSD camera head with its cooling system and readout electrics (preliminary design)

3. INFRARED WAVEFRONT SENSORS: THE E-APD RAPID REVOLUTION

3.1 Presentation of the RAPID HgCdTe e-APD array

Infrared HgCdTe Avalanche Photo Diodes (APD) have been show to exhibit single carrier multiplication (SCM) of electrons up to gains in the order of 10 000 associated with low excess noise factors F=1.05-1.4, record high gain-bandwidth product GBW>2.1THz and low dark currents. The technology used to manufacture APDs is similar to the one used for standard n on p HgCdTe diodes explaining why a high quantum efficiency (typically QE=80-95 %) is maintained from the visible wavelengths up to the infrared (IR) cut-off wavelength. They have inspired a large effort in developing focal plan arrays using HgCdTe APDs for low photon number applications such as active imaging in the range gated mode (2D) and/or with direct time of flight detection (TOF) (3D) and, more recently, passive imaging for wave front correction and fringe tracking in astronomical observations [24] funded by the RAPID programme.

The RAPID programme is a 4 years R&D project funded by the French "Fonds Unique Interministériel" in 2009. It includes several industrial and academic partners from the field of advanced infrared focal plane arrays fabrication (SOFRADIR [25], CEA-LETI) and of astronomical/defense institutes (IPAG, LAM, ONERA). The goal of this programme is to develop a fast and low noise infrared focal plane array of moderate format for astronomical fast application like adaptive optics wavefront sensing and fringe tracking for astronomical interferometers.

A similar development with a APD array of the same pixel format and pitch is also carried out by ESO and SELEX Galileo Infrared Ltd. (UK), all details of this development is given in [26].

The main characteristics of the infrared array developed in this programme are summarized in Table 7.

Table 7: the RAPID 320x256 1500 Hz infrared detector characteristics fabricated by SOFRADIR [25]

Characteristic	Requirement	Achievement
Pixels Format	320 x 256 pixels 30µm pitch	320 x 255 pixels 30µm pitch
Technology	HgCdTe	HgCdTe array with intra-pixel Correlated Double Sampling
Cut-off wavelength	3µm@77K	3µm @ 77K
Window	Rectangular window to speed up frame rate	A rectangular window can be defined with the start line and the end line of the window to be read.
Readout noise with gain	<2e- with gain x20	~ 34 e- with gain x1 3.4 e- with gain x10
Sensitivity	Visible to IR Cut-off	0.4 – 3 µm
APD Gain	x20	~x 10 @ 7V (limited by the readout circuit operation)
Max. frame rate	1500 Hz	Up to 2 000 Hz
Dark signal	4000 e-/s	6 750 e-/s measured, not limited by device but by setup background
Power consumption	210 mV	122 mW
Temperature operation	Liquid nitrogen	80K with liquid nitrogen of miniature cryocooler (Stirling, pulse tube)
Packaging	Detector packaged in a cryostat	Detector packaged in a cryostat with miniature pulse tube or Stirling cryocooler
Availability		Year 2013-2014 (SOFRADIR)

RAPID is a 320x256 infrared focal plane array based on the e-APD HgCdTe technology. The APD allows to apply moderate multiplication gain without adding noise, therefore lowering the readout noise without almost no penalty. This is the only way to obtain the fast frame rates needed by wavefront sensing with readout noise lower than 5 e. This kind of performances can not been achieved by classical HgCdTe arrays, the APD technology is absolutely necessary.

The ultimate goal of the RAPID development is to demonstrate operation of the 320x256 pixels 30 microns pitch infrared array at 2000 fps with 2 e- readout noise. To achieve such readout noise and fast frame rate, APDs technology and intra-pixel Correlated Double Sampling were both needed. The floor plan of the device is shown in the Figure 23, it includes 8 parallel outputs clocked at 20 MHz pixel rate defining 8 stripes of 40x256 pixels with one amplifier per stripe.

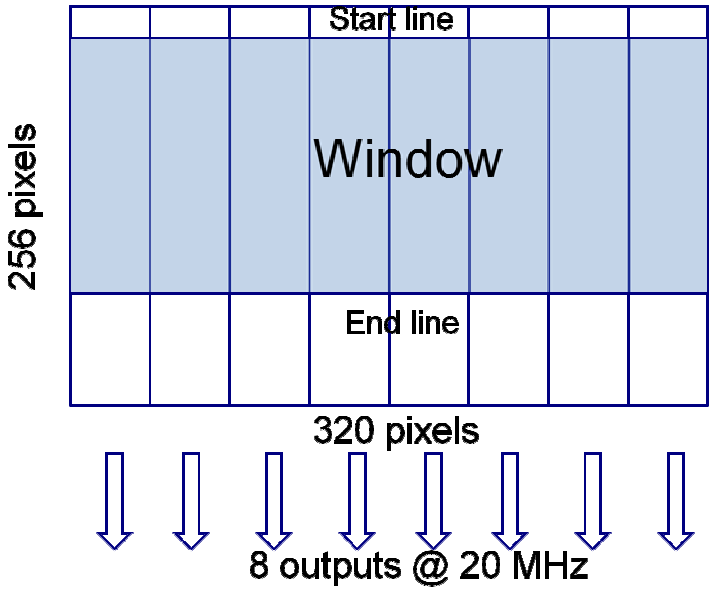

Figure 23: the 1.5 kfps RAPID e-APD infrared detector configuration: 8 outputs 320 x 256 pixels with 30 µm pitch. A rectangular window with programmable start line and end line can be defined to speed up the frame rate.

3.2 RAPID e-APD results

The Figure 24 and Figure 25 show a flat field of the RAPID array in front of a backbody allowing to compute the device operability at ±30%. For all good devices produced so far, the operability at 1.5 kfps is in the range 99.2-99.3% on the whole gain range from x1 to x10.

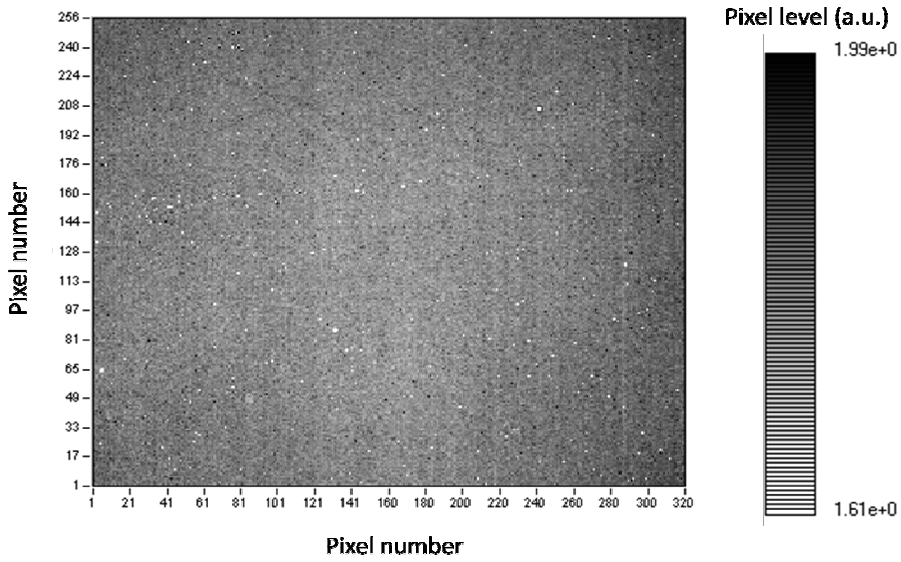

Figure 24: RAPID 320x256 e-APD flat field at 1500 fps with gain x6 showing 99.2% of operability at ±30%.

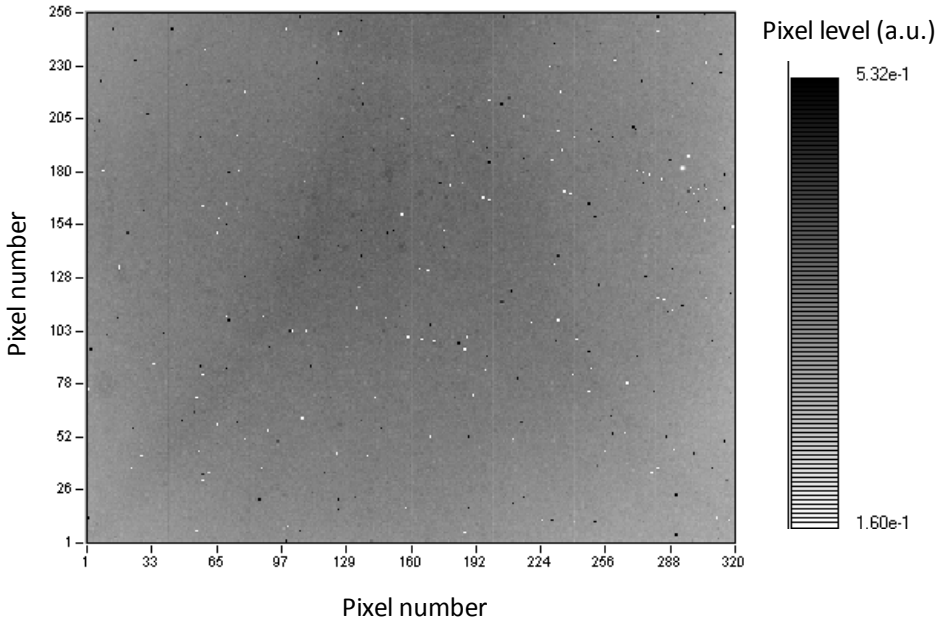

Figure 25: RAPID 320x256 e-APD flat field at 1500 fps with gain x10 showing 99.3% of operability at ±30%.

The multiplication gain of the APD mainly depends on the cut-off wavelength and the reverse bias voltage of the photodiode, also but with less sensitivity depends on the detector temperature. The gain increases with the bias voltage, the cut-off wavelength and decreases with the temperature.

The bias voltage of the photodiode, performed by the readout circuit, is driven by the CMOS technology used for the readout circuit. Increasing the cut-off wavelength increases the gain but also the dark signal and the need for colder temperature. A first trade-off of these constrains was to choose a cut-off wavelength of 3 µm with a CMOS technology well proven for SOFRADIR allowing a -7V reverse bias.

With these parameters, the RAPID detector multiplication gain has been measured, this is showed in the plot of the Figure 26.

The RAPID devices have been tested by SOFRADIR and LETI-LIR in a test cryostat showed in the Figure 27.

The readout noise has been measured in this cryostat. A readout noise of 34 e was measured for full frame images (320x256 pixels) at gain x1, and 3.4 e at gain x10 with 1.5 kHz frame rate.

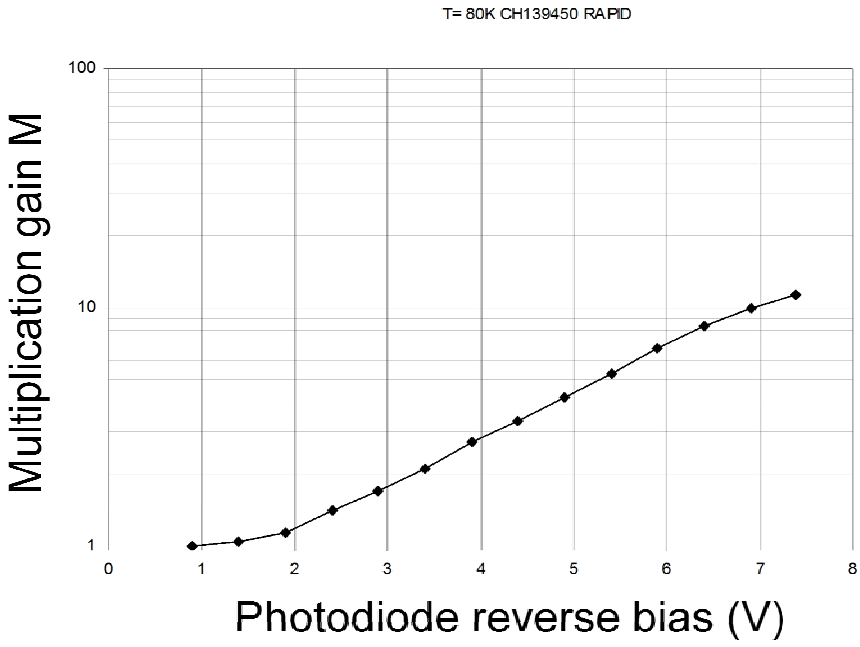

Figure 26: RAPID multiplication gain as a function of the photodiode reverse bias for 3 µm photodiodes cut-off at 80K.

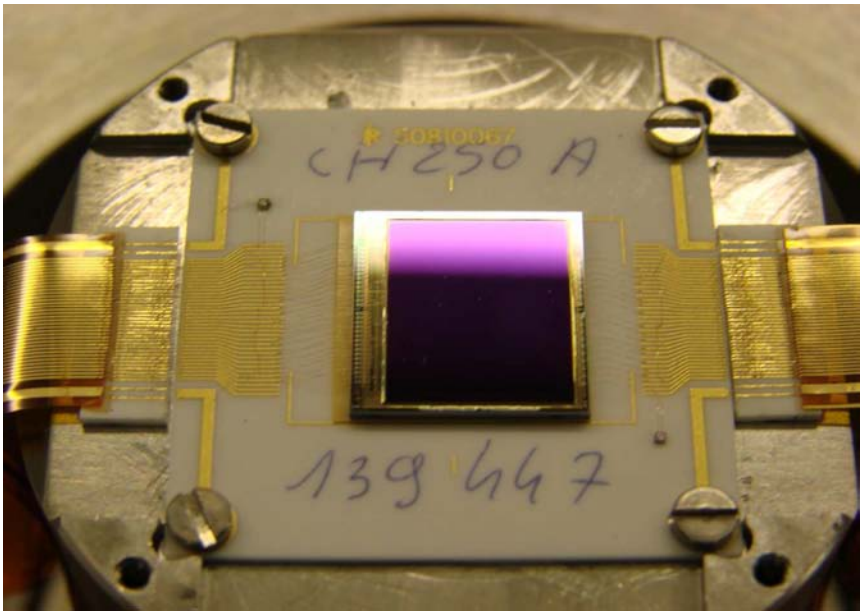

Figure 27: the 320x256 pixels RAPID infrared e-APD in the SOFRADIR detector test cryostat

3.3 Miniature nitrogen free cryostats developments for RAPID by Absolut System

For operation of the RAPID device on astronomical sites, a nitrogen free cryostat based on a miniature vibration free pulse tube fabricated by Absolute Systems SAS [27], see full description of this system in [28].

This miniature high power pulse tube under reference SSC80 is a custom Absolute Systems SAS development that provides 1.5 W of cooling power at 80K without almost no vibrations. This allows to have an extremely compact design of the cryostat in order to shorten the electrical wiring between the detector and the front end electronics to less than 5 cm (see Figure 30 and Figure 31). Low pass cold filters are used to reject high wavelengths background. The cold filters, cooled at 80K, are low pass filters with 1.9 µm cut-off. An additional floating screen, see Figure 31 (right), is also used to shield the cryostat background. It is anticipated that the short distances between the detector and the front end electronics will decrease the readout noise and will allow detector operation a 2 kHz frame rate with no penalty on the other performances.

A First Light Imaging [19] RAPID camera system based on the developments described above will also be commercially available in 2014.

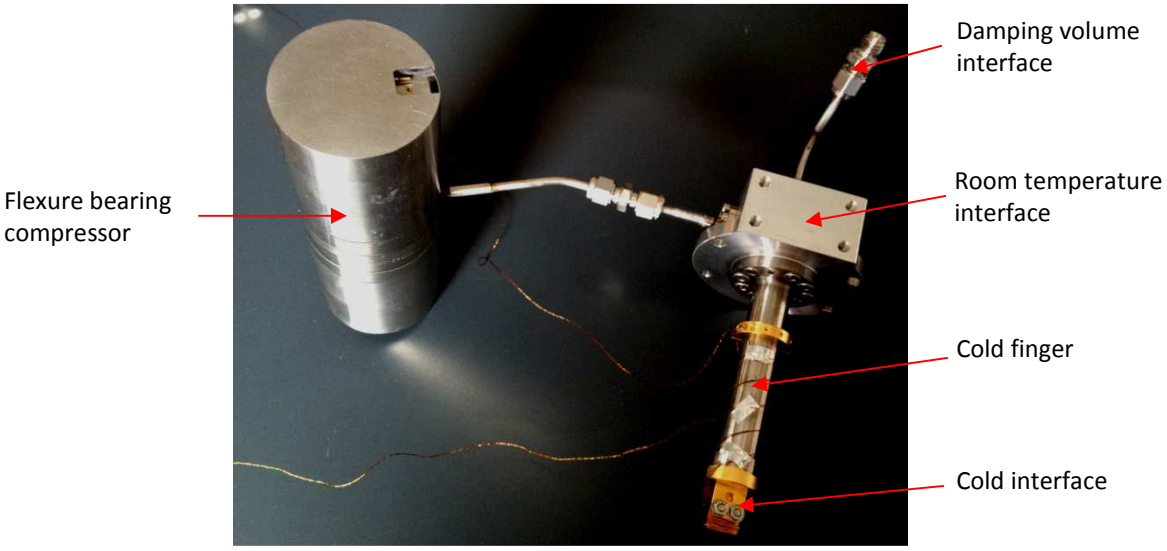

Figure 28: the Absolut Systems SSC80 no vibration high performance pulse tube custom development for RAPID detector cooling .

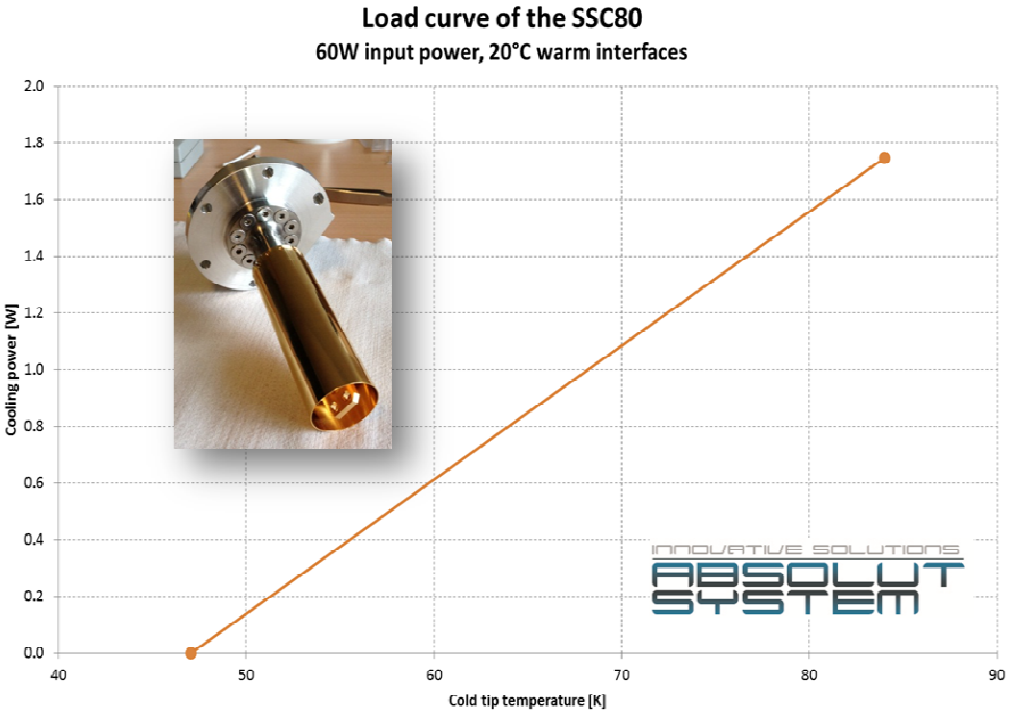

Figure 29: cooling power as a function of the temperature of the SSC80 miniature pulse tube developed for the RAPID infrared APD array by Absolut system [27], [28].

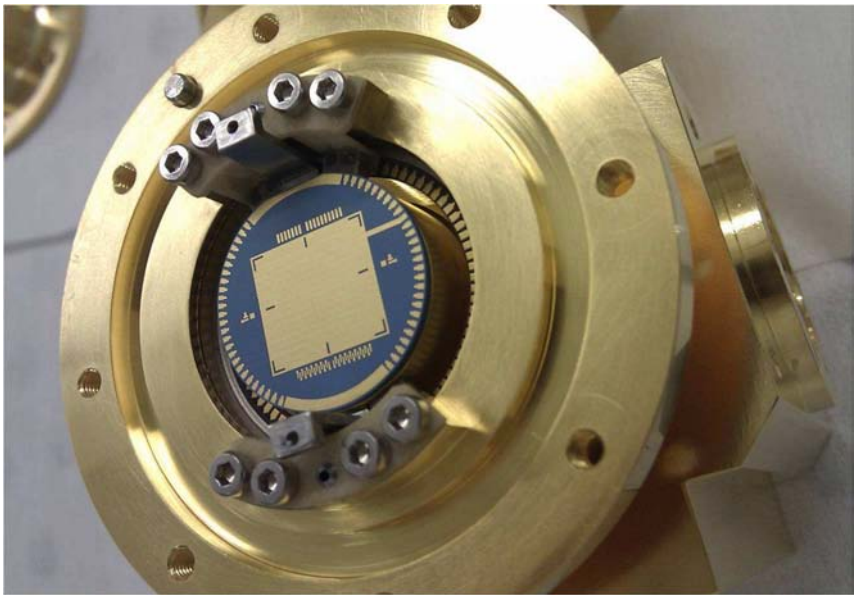

Figure 30: the RAPID cryostat with the cold ceramic before gluing the detector.

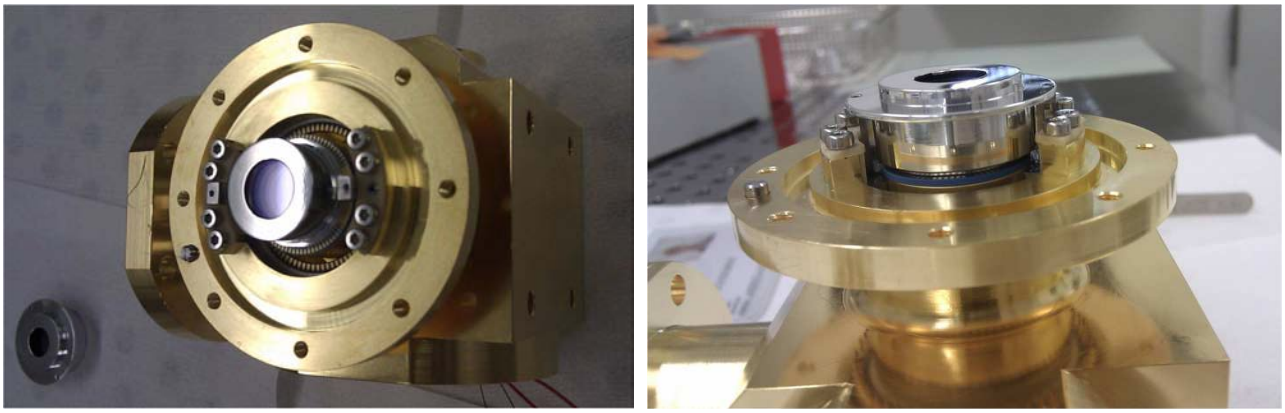

Figure 31: the RAPID cryostat with the cold filter (left) and with the additional floating shield (right).

3.4 Linear photon counting with HgCdTe APD at CEA-LETI Grenoble

Linear mode proportional photon detection has been demonstrated using HgCdTe APDs hybridized with a specially designed low noise ROIC [29]. The main objective of the ROIC design was to achieve an ultra low noise at intermediate BW (10 MHz) to demonstrate single photon detection at low to moderate gains (30-200), in order to obtain reduced Dark Count Rate (DCR) and /or increased operating temperature, but also to use the detector assembly to study the probability distribution function of the avalanche gain. The ROIC was also designed for low nominal power consumption (13 µW) and small footprint, which enables its integration into large area FPAs. The performance was found to be close to the nominal values in terms of gain (0.1 mV/electron), bandwidth (6 MHz) noise (10 electrons). The circuit was found to be linear up to 1000 electrons between two resets of the ROIC, i.e. the observation time. At a gain of 100 and using a fast reset time, the dynamic can be estimated to range between the DCR and 10 photons per observation time. In addition, the linear detection mode enables to increase the dynamic range by a temporal variation of the gain.

The detectors were tested using a gain switched semi-conductor laser which emits laser pulses with a typical duration of 40 ps and energy of 1.2 pJ (107 photons per pulse) at frequencies between 100 kHz to 1 GHz. The number of photons per impulse that impinges the detector was controlled by placing the fibre optic at a cm distance to the detector (typically 3 cm) and using a fibre coupled variable optical attenuator (VOA). At zero attenuation, the divergence of the beam at the output of the single mode fibre leads to about 300 photons per pulse on the pixel of 30x30 µm. Hence, an optical attenuation of the order of 100 yields close to unity photon number states.

Proportional photon counting has been demonstrated using a MWIR and SWIR HgCdTe APDs. The Poison statistics of a pulsed laser light was reproduced for average photon number states of m=0.8 to 8, demonstrating the capability of detecting single or multiple photons using linear mode APDs for APD gains ranging from gain M=40 to 200.

The capability of single photon detection and proportional photon counting was characterized by measuring the amplitude distribution of the step response that occurs, with and without laser illumination, at the expected instant of detection of the laser impulse. The measurements were made with MWIR HgCdTe APDs using the buffered detector assembly (APD type *b*) at APD gains varying between 40 and 200.

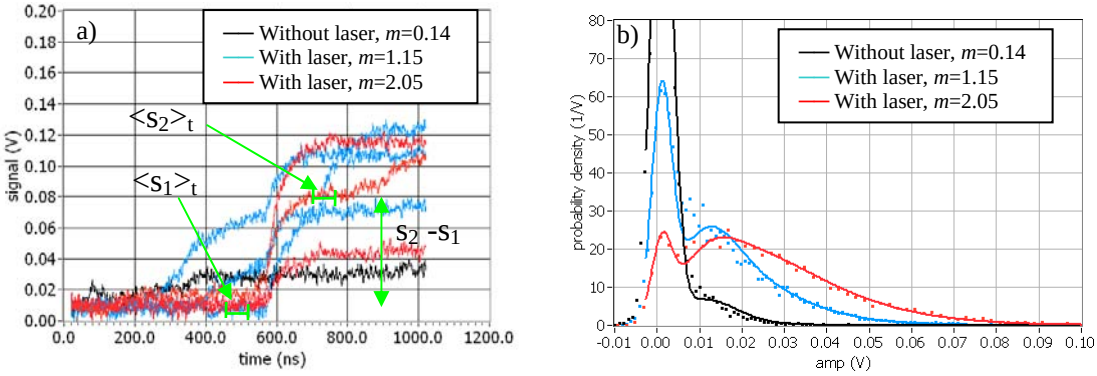

Figure 32 a) output signal without and with laser illumination (for two conditions of attenuation). The arrows indicates the position of the s_2 and s_1 estimators. b) Measured Probability Density Functions (PDF) for the step amplitude (dots) compared with calculated Poisson distributions for average photon number m=0.14 (without laser), 1.15, 2.05. The measurements were performed at substrate bias of -8V (APD reverse bias of 8.7 V) at 80 K. From [29].

The probability density corresponding to the detection of one or several photons is well distinguished from the zero photon distribution, see Figure 32b) implying that single photon detection can be achieved at threshold values below the average gain value for a single photon and, as a consequence, with a high Photon Detection Efficiency (PDE). As the input flux is not controlled in this experiment, it is not possible to quantify the external PDE in this experiment. An approximate calculation of the internal PDE is proposed below by the analysis of the amplitudes of the residual thermal photons. A difference between the measured and calculated PDFs is however observed at m=1.15, between the average zero and single photon peaks, where the experimental densities are higher and do not present a minimum. A similar behavior is observed at m=2.05, even though the differences is lower in this case.

The present results confirm the high potential in using HgCdTe APD for linear mode photon counting. The low noise ROIC do not only allow to demonstrate photon counting at moderate gain values, which should enable reduced DCR and/or increased operating temperature. Further experiments are required to confirm the estimated values of the PDE and DCR, using a single photon source and at zero flux. The present work will also be pursued by the characterization of devices with optimized APD performance, in terms of gain excess noise and dark currents (which should yield DCR values in the range of 10 Hz), and by the development and/or testing of devices with other ROICs. In particular, the present amplification stage will be tested with an integrated thersholding circuit and the present design could benefit from an optimization of the bandwidth, while conserving a low noise, with the ultimate objective to approach the fundamental limit in response time and jitter, which should be lower than 100 ps.

4. CONCLUSION

For the first time, the CCD220 and OCAM2 have demonstrated sub-electron noise for a 240x240 pixel camera system running at 1300 frames per second with the detector operated at a temperature of -40°C. This paper reports on the comprehensive, quantitative performance characterization of OCam and the CCD220 such as readout noise, dark current, multiplication gain, quantum efficiency, charge transfer efficiency. The CCD220 is a new detector fabricated by *e2v technologies* [5] based on their L3Vision technology. It includes 8 outputs, split frame transfer architecture to lower detector smearing while the detector is read, 8 L3Vision registers to have multiplication gain and sub-electron noise at high speed. Both developed within the European OPTICON network [3], the CCD220 detector and the OCam camera were designed for AO applications with optimized performances in terms of noise and frame rate. A deep depleted variant of the CCD220 also exists with same overall performances and improved QE in the red.

A world record of 0.48 e mean RMS Noise was achieved with the 240x240 pixels CCD220 at 1500 frames per second and gain x200 (0.16 e with gain x600). Under these conditions, the dark current is <0.01 e/pixel/frame and the peak QE is 94% at 650 nm wavelength due to back-thinning and back-illumination of the CCD. This achievement is a major

breakthrough in the field of wavefront sensing for advanced Adaptive Optics systems to be used in the next generation of ground based telescope instruments.

A production camera, called OCAM2 and based on OCam experience, is designed and commercialized by First Light Imaging [19] to run at 1500 fps without degrading OCam performances. OCAM2 has been designed to be ruggedized and can accept more demanding environmental conditions. Ready to use, OCAM2 is designed for reliable operation on a telescope. Custom microlens array integration can easily be performed based on a flexible mechanical design of the front cover and past experience of microlens integration in the most advanced existing AO systems. A future development will start soon to speed up the frame rate of OCAM2 up to 2500 Hz in order to accommodate the most demanding future AO applications.

Additional wavefront sensing detector developments are now carried out in Europe for next generation of telescope. A long programme has started in 2004 for developing large CMOS detectors for the E-ELT with several phases, all detectors are fabricated by e2v. The current phase consist in the production of a 880x800 pixel fully digital CMOS detector which should provide 3 e- read noise at 700 Hz (1000 Hz with degraded performances) and optimal QE. This detector, called NGSD, will be used for natural and laser guide start systems on Extremely Large Telescopes. A camera system based on the NGSD, commercialized by First Light Imaging, will be offered by 2014. A larger device development with same characteristics except a detector size of 1760x1680 will start in a next phase. Infrared wavefront sensors, called RAPID and based on a 2 kfps 320x256 pixels infrared APD arrays, are also currently produced and tested already demonstrating read noise lower than 4e at this frame rate (goal 2e). This infrared detector is produced by SOFRADIR [25]. Again, a commercial camera based on this innovating detector will be commercialized by First Light Imaging [19].

This paper illustrates a long term and coordinated wavefront sensor development involving cutting edge detectors and camera systems industry associated with ESO and academic French laboratories (LAM, IPAG and OHP).

ACKNOWLEDGEMENTS

These developments have been partly carried out using OPTICON and FUI funds.

OPTICON is supported by the European Commission's FP7 Capacities programme (Grant number 226604).

The RAPID programme is funded by the Fonds Unique Interministériel (FUI) under the 7th AAP from the French "Ministère de l'Economie, des Finances et de l'Emploi".

Funding is also: ESO, CNRS, Université de Provence, Sofradir, ONERA and CEA/LETI.

REFERENCES

[1] Moorwood, A., "Instrumentation at the ESO VLT ", Proc. SPIE 6269, 626904 (2006).
[2] Feautrier, P., Kern, P. Y., Dorn, R. J., Rousset, G., Rabou, P., Laurent, S., Lizon, J., Stadler, E., Magnard, Y., Rondeaux, O., Cochard, M., Rabaud, D., Delboulbe, A., Puget, P., Hubin, N. N., "NAOS visible wavefront sensor" in *Adaptive Optical Systems Technology*, edited by Peter L. Wizinowich, Proceedings of SPIE Vol. 4007, pp. 396-407 (2000).
[3] Gillmore, G. F., "OPTICON: a (small) part of European astronomy", Proc. SPIE 5382, 138 (2004).
[4] Feautrier, P., Fusco, T., Downing, M., Hubin, N., Gach, J-L., Balard, P., Guillaume, C., Stadler, E., Boissin, O., Jorden, P., Diaz, J-J., "Zero noise wavefront sensor development within the Opticon European network", Scientific Detectors for Astronomy 2005, Springer Netherlands editor, ISBN: 978-1-4020-4329-1, Beletic, Jenna E.; Beletic, James W.; Amico, Paola (Eds.), Vol. 336 (2006).
[5] e2v technologies, http://www.e2v.com/.
[6] Jerram, P., Pool, P. J., Bell, R., Burt, D. J., Bowring, S., Spencer, S., Hazelwood, M., Moody, I., Catlett, N. and Heyes, P. S., "The LLCCD: low-light imaging without the need for an intensifier", in Proc. SPIE, 4306, pp. 178-186, May 2001.

[7] Fusco, T., Nicolle, M., Rousset, G., Michau, V., Beuzit, J-L, Mouillet, D., "Optimisation of Shack-Hartman based wavefront sensor for XAO systems", Advancements in Adaptive Optics. Edited by Domenico B. Calia, Brent L. Ellerbroek, and Roberto Ragazzoni. Proceedings of the SPIE, Volume 5490, pp. 1155-1166 (2004).
[8] Robbins, M., Hadven, B., "The Noise Performances of Electron Multiplying Charge-Coupled Devices", IEEE Transactions On Electron Devices, Vol. 50, No. 5, pp. 1227-1232 (2003).
[9] Petit, C., Fusco, T., Charton, J., Mouillet, D., Rabou, P., Buey, T., Rousset, G., Sauvage, J.-F. , Baudoz, P. , Gigan, P., Kasper, M., Fedrigo, E., Hubin, N., Feautrier, P. , Beuzit, J.-L., Puget, P. , "The SPHERE XAO system: design and performance", Proc. SPIE 7015, 70151D (2008).
[10] Beuzit, J., Feldt, M., Dohlen, K., Mouillet, D., Puget, P., Wildi, F., Abe, L., Antichi, J., Baruffolo, A., Baudoz, P., Boccaletti, A., Carbillet, M., Charton, J., Claudi, R., Downing, M., Fabron, C., Feautrier, P., Fedrigo, E., Fusco, T., Gach, J., Gratton, R., Henning, T., Hubin, N., Joos, F., Kasper, M., Langlois, M., Lenzen, R., Moutou, C., Pavlov, A., Petit, C., Pragt, J., Rabou, P., Rigal, F., Roelfsema, R., Rousset, G., Saisse, M., Schmid, H., Stadler, E., Thalmann, C., Turatto, M., Udry, S., Vakili, F., Waters, R., "SPHERE: a planet finder instrument for the VLT" in Ground-based and Airborne Instrumentation for Astronomy II, edited by Ian S. McLean, Mark M. Casali, Vol. 7014, 701418 (2008).
[11] Downing, M., Kolb, J., , Baade, D., Iwert, O., Hubin, N., Reyes, J., Feautrier, P., Gach, J-L., Balard, P., Guillaume, C., Stadler, E., Magnard, Y., "AO Wavefront Sensing Detector Developments at ESO", Proc. SPIE 7742-4, San Diego, (2010).
[12] Feautrier, P., Gach, J., Balard, P., Guillaume, C., Downing, M., Stadler, E., Magnard, Y., Denney, S., Suske, W., Jorden, P., Wheeler, P., Skegg, M., Pool, P., Bell, R., Burt, D., Reyes, J., Meyer, M., Hubin, N., Baade, D., Kasper, M., Arsenault, R., Fusco, T., Diaz Garcia, J. J., "The L3Vision CCD220 with its OCam test camera for AO applications in Europe" in High Energy, Optical, and Infrared Detectors for Astronomy III, edited by David A. Dorn, Andrew D. Holland, Proceedings of SPIE Vol. 7021, 70210C (2008).
[13] Downing, M., Finger, G., Baade, D., Hubin, N., Iwert, O., Kolb, J., "Detectors for AO wavefront sensing", Proc. SPIE 7015, 70151R (2008).
[14] Downing, M., Hubin, N., Kasper, M., Jorden, P., Pool, P., Denney, S., Suske, W., Burt, D. Wheeler, P., Hadfield, K., Feautrier, P., Gach, J-L, Reyes, J., Meyer, M., Baade, D., Balard, P. Guillaume, C., Stadler, E., Boissin, O., Fusco, T., Diaz, J-J., "A Dedicated L3Vision CCD for Adaptive Optics Applications", Scientific Detectors for Astronomy 2005, Springer Netherlands editor, ISBN: 978-1-4020-4329-1, Beletic, Jenna E.; Beletic, James W.; Amico, Paola (Eds.), Vol. 336 (2006).
[15] Downing, M., Arsenault, R., Baade, D., Balard, P., Bell, R., Burt, D., Denney, S., Feautrier, P., Fusco, T., Gach, J., Diaz Garcia, J. J., Guillaume, C., Hubin, N., Jorden, P., Kasper, M., Meyer, M., Pool, P., Reyes, J., Skegg, M., Stadler, E., Suske, W., Wheeler, P., "Custom CCD for adaptive optics applications" in *High Energy, Optical, and Infrared Detectors for Astronomy II*, edited by David A. Dorn, Andrew D. Holland, Proceedings of SPIE Vol. 6276, 62760H (2006).
[16] Reyes, J., Conzelman, R., "ESO AO Wavefront Sensor Camera", Detectors for Astronomy 2009 workshop, http://www.eso.org/sci/meetings/dfa2009/, ESO Garching, 12-16 October (2009).
[17] Gach, J-L., Balard, P., Boissin, O., Downing, M., Feautrier, P., Guillaume, C., Stadler, E. , "A dedicated controller for Adaptive Optics L3CCD developments", Scientific Detectors for Astronomy 2005, Springer Netherlands editor, ISBN: 978-1-4020-4329-1, Beletic, Jenna E.; Beletic, James W.; Amico, Paola (Eds.), Vol. 336 (2006).
[18] Feautrier, P., Stadler, E., Downing, M., Hurrell, S., Wheeler, P., Gach, J., Magnard, Y., Balard, P., Guillaume, C., Hubin, N., Diaz, J. J., Suske, W., Jorden, P., "Thermal modelling of cooled instrument: from the WIRCam IR camera to CCD Peltier cooled compact packages" in *Modeling, Systems Engineering, and Project Management for Astronomy II*, edited by Martin J. Cullum, George Z. Angeli, Proceedings of SPIE Vol. 6271, 62710S (2006).
[19] First Light Imaging, www.firstlight.fr
[20] Robbins, M., "Estimating Ultra Low Levels of Dark Signal Using an L3Vision Device", e2v technical note, Doc. L3V-TN-635, http://www.e2v.com, (2005).
[21] Javier Reyes Moreno, Mark Downing, Ralf D. Conzelmann, Mirko Todorovic, Joerg Stegmeier, " An overview of the ESO adaptive optics wavefront sensing camera", Proc. SPIE Astronomical Telescopes + Instrumentation, [8447-237], Amsterdam (2012).
[22] Mark Downing, Johann Kolb, Gert Finger, Olaf Iwert, Norbert Hubin, Javier Reyes, Philippe Feautrier, Jean-Luc Gach, Philippe Balard, Christian Guillaume, Eric Stadler, Martin Fryer, Paul Jorden, Andrew Walker,

Andrew Pike, Paul Jerram, Jerome Pratlong, Bart Dierickx, Benoit Dupont, Arnaud Defernez, "Backside-Illuminated, high QE, 3e- RoN, fast 700fps, 1760x1680 pixels CMOS Imager for AO with highly parallel readout", Proc. SPIE Astronomical Telescopes + Instrumentation, [8453-12], Amsterdam (2012).

[23] Downing, M., et. al., “Review of AO Wavefront Sensing Detectors”, DfA Garching (2009), http://www.eso.org/sci/meetings/dfa2009/Writeups/WR-Downing_A0WFS_DfA2009.pdf.

[24] J. Rothman et al., accepted for publication in *J. Electron. Mater*., **41**, (2012) : DOI: 10.1007/s11664-012-1970-4;

[25] SOFRADIR, http://www.sofradir.com

[26] Gert Finger, Ian M. Baker, Derek J. Ives, Siegfried Eschbaumer, Leander H. Mehrgan, Manfred Meyer, Joerg Stegmeier, Peter Thorne, Harald J. Weller, "Evaluation and optimization of NIR HgCdTe avalanche photodiode arrays for adaptive optics and interferometry", Proc. SPIE Astronomical Telescopes + Instrumentation, [8453-30], Amsterdam (2012).

[27] Absolut Systems SAS, 32 rue de la Tuilerie, 38170 Seyssinet-Pariset, France, contact@absolut-system.com.

[28] J. Tanchon, T. Trollier, Y. Icart, A. Ravex, P. Feautrier, Eric Stadler, "Small Scale 80K Pulse Tube Cooler for RAPID e-APD infrared Camera", Proceedings of Cryocoolers 17, edited by S. D. Miller and R. G. Ross, Jr.

[29] Gautier Vojetta, Fabrice Guellec, Lydie Mathieu, Kevin Foubert, Philippe Feautrier and Johan Rothman, "Linear photon-counting with HgCdTe APDs", Proc. SPIE 8375, 83750Y (2012);